

# Branching archaeocyaths as ecosystem engineers during the Cambrian radiation

Ryan A. Manzuk<sup>1</sup>  | Adam C. Maloof<sup>1</sup>  | Jaap A. Kaandorp<sup>2</sup>  | Mark Webster<sup>3</sup> 

<sup>1</sup>Department of Geosciences, Princeton University, Princeton, New Jersey, USA

<sup>2</sup>Computational Science Lab, University of Amsterdam, Amsterdam, The Netherlands

<sup>3</sup>Department of the Geophysical Sciences, University of Chicago, Chicago, Illinois, USA

## Correspondence

Ryan A. Manzuk, Department of Geosciences, Princeton University, Princeton, NJ 08544, USA.  
 Email: [rmanzuk@princeton.edu](mailto:rmanzuk@princeton.edu)

## Funding information

National Science Foundation; Princeton University

## Abstract

The rapid origination and diversification of major animal body plans during the early Cambrian coincide with the rise of Earth's first animal-built framework reefs. Given the importance of scleractinian coral reefs as ecological facilitators in modern oceans, we investigate the impact of archaeocyathan (Class Archaeocyatha) reefs as engineered ecosystems during the Cambrian radiation. In this study, we present the first high-resolution, three-dimensional (3D) reconstructions of branching archaeocyathide (Order Archaeocyathida) individuals from three localities on the Laurentian paleocontinent. Because branched forms in sponges and corals display phenotypic plasticity that preserve the characteristics of the surrounding growth environment, we compare morphological measurements from our fossil specimens to those of modern corals to infer the surface conditions of Earth's first reefs. These data demonstrate that archaeocyaths could withstand and influence the flow of water, accommodate photosymbionts, and build topographically complex and stable structures much like corals today. We also recognize a stepwise increase in the roughness of reef environments in the lower Cambrian, which would have laid a foundation for more abundant and diverse coevolving fauna.

## KEY WORDS

archaeocyath, biodiversity, Cambrian, coral, ecosystem engineering, paleoenvironment, reef, sponge, three-dimensional

## 1 | INTRODUCTION

The early Cambrian (Terreneuvian and Epoch 2; 539 to 509 million years ago) saw the first appearance and radiation of diverse communities of robust, skeletonized animals (Erwin & Valentine, 2012; Lipps & Signor, 1992; Zhuravlev & Riding, 2001). This unique interval is a landmark in the evolution of life on Earth, and so workers have sought to constrain the marine environmental conditions that may have contributed to the high rate and magnitude of evolutionary innovation. Much of the research in this area has investigated [A] chemical environmental change like oxygenation (Berkner & Marshall, 1965; Canfield et al., 2007; Catling et al., 2005; Dahl et al., 2019) or nutrient fluxes (Brasier & Lindsay, 2001; Peters & Gaines, 2012; Squire et al., 2006), [B] novel ecological feedbacks (Bottjer et al., 2000;

Cloud, 1968; Meysman et al., 2006; Vermeij, 1989), and [C] genetic and developmental innovations (Brooke et al., 1998; Peterson et al., 2009; Valentine, 1986). In terms of the physical environment available to animals during the early Cambrian, past work largely has focused on an increase in continental shelf area, providing more shallow seafloor for metazoan communities, especially in the tropics (Brasier & Lindsay, 2001; Peters & Gaines, 2012; Valentine & Moores, 1972). However, another potential shift in the physical characteristics of shelfal environments likely occurred due to the rise of Earth's first framework reefs built by calcifying animals—the archaeocyath sponges (Class Archaeocyatha). To date, studies of these reefs have focused on taxonomy, paleoecology, and biostratigraphy (Antcliffe et al., 2019; Debrenne, 2007; Erwin & Tweedt, 2012; Pratt et al., 2001; Pruss et al., 2012, 2021; Rowland & Gangloff, 1988;

Wood et al., 1992; Zhuravlev, 2001; Zhuravlev & Wood, 1995), but the substrate geometries of these structures and their potential environmental impacts have yet to be constrained.

## 1.1 | The environmental importance of reefs

In both ancient and modern oceans, metazoan reefs serve as biodiversity hotspots (Idjadi & Edmunds, 2006; Kiessling et al., 2010). Multiple qualities of reefs act to increase local animal abundance and diversity (Reaka-Kudla, 1997), and one important factor is topographic complexity, or roughness (Kostylev et al., 2005; Monismith, 2007). By providing a topographically complex surface, reefs increase the available habitat space over an area of seafloor, creating the framework for a denser and more diverse community with increased opportunity for organism interactions that promote speciation (Hatcher, 1988; Kostylev et al., 2005). Reef structure also can support a multitude of cavities where organisms take advantage of filtered light, redox gradients, and physical refugia that otherwise would not be available in the near surface (Kobluk, 1988). These unique habitats, along with associated photosymbionts, add pathways to enhance reef trophodynamics, increasing both the production and consumption of organic matter (Richter & Wunsch, 1999).

In addition to providing physical spaces, a rough reef surface alters local fluid boundary layer conditions at multiple scales. A reef in its entirety will disrupt the benthic boundary layer, localizing sedimentation, erosion, and nutrient flux to and from continent-derived and open-ocean waters (Shashar et al., 1996). The smaller-scale roughness added by densely branching corals on a reef's surface can shape the momentum and diffusive boundary layers to create pockets of quiescent waters, along with localized increases in current velocity that enhance chemical fluxes across thinned diffusive boundaries (Monismith, 2007; Shashar et al., 1996; Thomas & Atkinson, 1997). These fluid boundary layer dynamics also create favorable conditions for nutrient absorption, suspension feeding, photosynthesis, prey capture, and larvae dispersal (Monismith, 2007; Shashar et al., 1996).

## 1.2 | Limits on interpretation of fossil reefs

Identifying the environmental and ecological importance of fossil reefs is not trivial. The geologic record is a biased and uneven chronicle of reef abundance and volume through time (Kiessling, 2005, 2006). Although there are known fossil examples of large barrier reef complexes (e.g., Kerans & Tinker, 1999; Playford, 1980), these structures are unlikely to be sampled at outcrop (James & Mountjoy, 1983) because they are narrow, only accounting for ~0.01% and 2% of current aerial extent on the Great Bahama Bank (Geyman & Maloof, 2021) and the Belize shelf (Purdy & Gischler, 2003), respectively. Furthermore, the platform margins occupied by barrier reefs are the most likely component

to be deformed or destroyed during orogenesis, biasing the record against their preservation (James & Mountjoy, 1983). Even indirect evidence of reefs, such as debris beds containing framework builders, are not likely to form major parts of the record because wave and bioerosion pulverize large skeletons before long-distance transport, most of which is in the direction of the foreslope (Land, 1979; Maxwell et al., 1961). In reef mounds that are preserved, up to 90% of the framework builders and associated taxa are turned to rubble or are recrystallized due to the coarse and porous nature of reefal sediments (Hubbard et al., 1990, 2001; Wood, 1999). Additionally, the contribution of soft-bodied and unpreserved taxa cannot be constrained in the geologic record (Signor, 1990). Thus, ecological studies of even Recent fossil reefs cannot recover the full biodiversity once present (Wood, 1999), and reconstructing ancient reef environments is restricted to a few, well-preserved examples (Hubbard et al., 2001).

In the lower Cambrian, archaeocyathan reefs most commonly are reported as small; sometimes, isolated patch reefs replete with calcimicrobes (Figure 1b,e; Debrenne, 2007; Pruss et al., 2012; Rowland & Gangloff, 1988). Within these reefs, paleoecological studies have noted a well-developed cryptobiota, potentially taking advantage of crevices and vugs (Hicks, 2001; Kobluk & James, 1979; Zhuravlev & Wood, 1995), as well as endemic faunas reliant on reefal environments (Pratt et al., 2001; Zhuravlev et al., 2015; Zhuravlev & Naimark, 2005). However, most studies conclude that Cambrian reef-dwelling faunas were depauperate, leaving the connection between archaeocyathan reefs and the Cambrian radiation ambiguous (Cordie et al., 2019; Rowland & Shapiro, 2002). Given the uncertainties and biases in assessing reef paleoecology, this set of observations might underestimate the impact of archaeocyathan ecosystem engineering on lower Cambrian biodiversity (Cordie et al., 2019).

Small patch reefs are not the only archaeocyath-built structures in the record. A site in the Yukon, Canada does preserve several large reefs (Read, 1980) that each are over 300 m long, greater than 50 m in stratigraphic thickness, and show evidence of at least 5 m of synoptic relief (Figure 2b). This site, which we study herein, demonstrates that archaeocyaths were organisms capable of building large barriers that might have been prevalent (although not often preserved) in the early Cambrian. Given that archaeocyaths could build structures that spanned the same size range as modern coral reefs, it is perhaps surprising that fossil occurrence data do not suggest that these reefs were biodiverse habitats for major Cambrian radiation taxa (Cordie et al., 2019; Rowland & Shapiro, 2002). Were these reef environments crucial hosts to many Cambrian animals, but sampling or preservation bias—especially for soft-bodied taxa—lead to paleoecologies that underestimate their biodiversity (Cordie et al., 2019)? Or should we read these data at face value and conclude that early animals had not yet adapted to take advantage of reef structures (Cordie et al., 2019)? Instead of attempting to reconstruct paleoecology, we adopt another approach focused on the physical characteristics of Cambrian reef environments through detailed three-dimensional

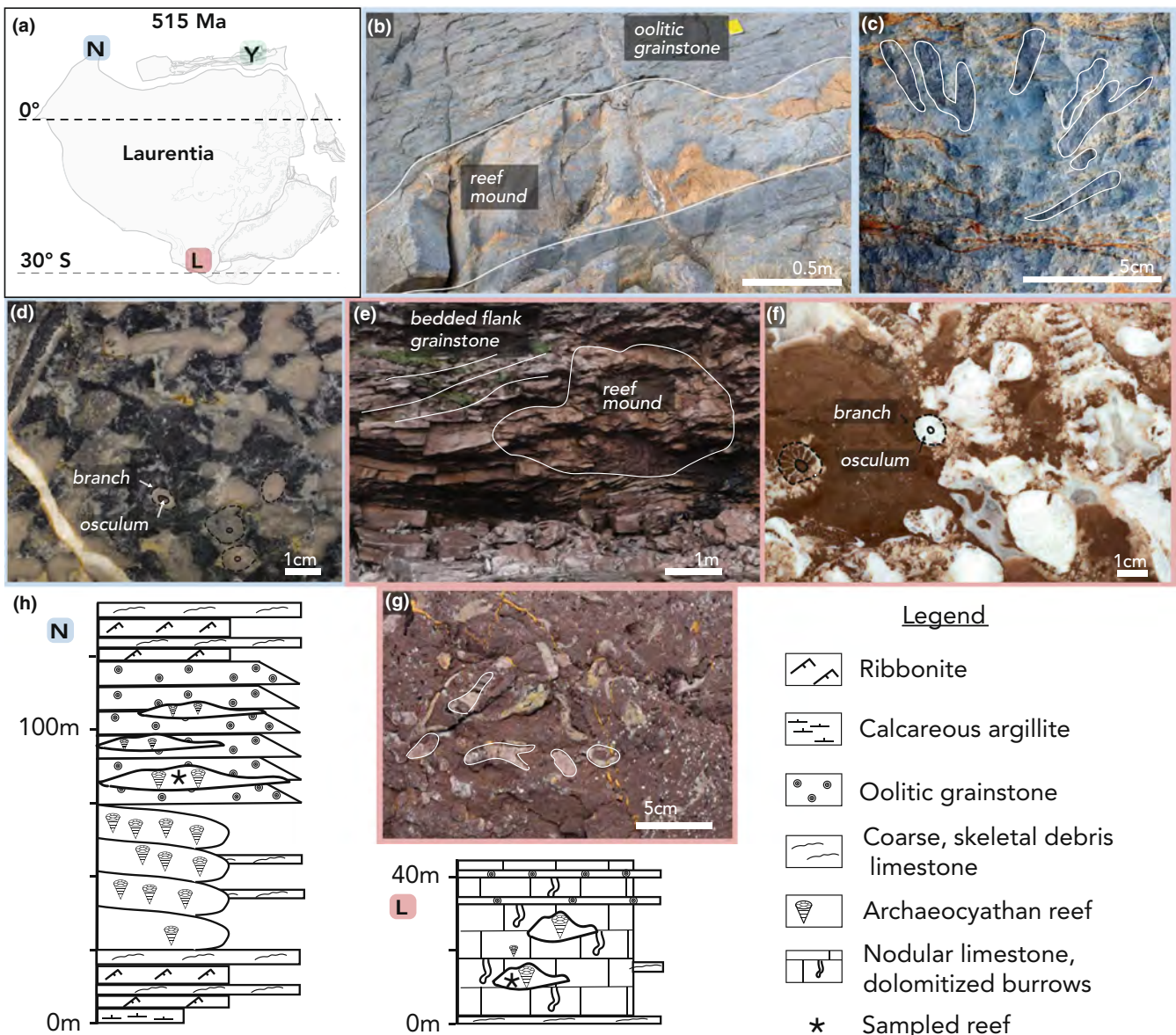


**FIGURE 1** Archaeocyathan reef examples and their paleogeography. (a) Laurentia reconstruction after Torsvik and Cocks (2016) and Domeier (2018), with field localities indicated (N = Nevada, Y = Yukon, L = Labrador). (b) Example of ~1 m-high reef at the Stewart's Mill, NV site where the variably dolomitized mound is preserved within an oolitic grainstone, indicating a shallow, wave-agitated environment. (c) The reefs preserved within the oolitic interval at the Nevada site contain *in situ* branching archaeocyathids, sometimes visible in the field (d) Example Grinding, Imaging, and Reconstruction Instrument (GIRI) output from the Nevada irregular archaeocyathide sample, with example traces of branches and oscula. (e) Three-dimensional rendering of Labrador outcrop containing archaeocyathid reefs and surrounding flank beds, produced using a structure-from-motion approach with handheld field photographs. (f) Example GIRI output of the Labrador archaeocyathide sample. (g) Close-up image of densely associated archaeocyathides surrounded by other skeletal material, typical of the Labrador site. (h) Generalized stratigraphic sections for the Nevada and Labrador Localities. See text for discussion.

(3D) analysis of branching archaeocyaths. Here, we are asking: were archaeocyaths morphologically analogous to scleractinian corals, such that the reefs they built would have small-scale characteristics (e.g., surface roughness) that could support a dense and diverse community of animals? Or do archaeocyath morphologies indicate that Cambrian reefs were entirely different environments from modern coral reefs, and the relatively low sampled diversity of associated taxa should be expected given surface characteristics that were not amenable to supporting a higher diversity?

### 1.3 | The need for 3D data in studies of ancient reefs

One of the most powerful tools for overcoming the problem of incomplete preservation in geology and paleobiology is detailed comparison between the best-preserved portions of the record and a modern analog. In the case of fossil reefs, well-preserved portions sometimes host evidence of *in situ* growth and attachment of calcifying organisms that offer insights toward past biological and environmental surface

conditions. Workers taking this approach in analyses of two-dimensional (2D) cross-sections of archaeocyathan reefs have recognized encrustation, anastomosis, and competitive overgrowth (James et al., 1977; Pratt et al., 2001; Wood et al., 1992; Zhuravlev & Wood, 1995). These observations suggest that space was a limiting resource in Cambrian reefs, and that structural interlocking of skeletal elements could have provided a wave-resistant framework (James et al., 1977; Rees et al., 1989; Wood et al., 1992; Zhuravlev & Wood, 1995).

While 2D methods have constrained some aspects of archaeocyathan reefs, they do not allow quantitative comparison to modern reef-building corals. 3D measurements of branching coral colonies form a major part of our current understanding of modern reef surface characteristics in terms of flow regime (Monismith, 2007; Reidenbach et al., 2006), physical habitat spaces (Vytöpil & Willis, 2001), and accommodation of photosymbionts (Kaandorp et al., 2005). Much of this understanding stems from the fact that branching morphologies do not arise in corals and sponges through genetic mechanisms, but instead through phenotypic plasticity (Kaandorp, 2013; Shaish et al., 2007; Todd, 2008) that reflects the environmental influences on the accretion of their calcium carbonate skeletons (Kaandorp et al., 2005). Thus, the physics and chemistry of modern reef surfaces are imprinted in morphological metrics of corals, such as branching angle and spacing. Branched forms have been noted in archaeocyaths, especially within the archaeocyathides (Order Archaeocyathida; Rowland, 1984; Rowland & Gangloff, 1988; Wood et al., 1992), and although not all corals nor archaeocyaths branch, we specifically target these forms because they best display phenotypic plasticity. In this study, we produce the first 3D morphological data from modular archaeocyathide specimens, and leverage the analogy with modern corals to interpret the surface characteristics of Earth's first metazoan reefs.

## 2 | MATERIALS AND METHODS

### 2.1 | Geological setting

In Nevada, archaeocyathan reefs are preserved in the carbonate-rich lower member of the Poleta Formation at a locality commonly referred to as Stewart's Mill (Figure 1a–c; GPS: 37.430970, -117.458792, WGS84; Rowland, 1984; Rowland & Gangloff, 1988). The Poleta Fm at Stewart's Mill dips ~35° to the northwest and begins with approximately 20 m of bedded carbonate mudstones with occasional interbedded skeletal packstones. Above the bedded interval are ~50 m of a lower reef complex (Rowland et al., 2008) consisting of massive, *Renalcis*-dominated boundstones with few (~3% estimated volume) archaeocyaths of diverse morphology visible in the field (Figure 1g; Rowland & Gangloff, 1988). In this lower reef interval, reef flanks occasionally are draped with argillites with interbedded skeletal grainstones. These microbe-dominated reefs then transition upward into ~40 m of coarse oolitic grainstone and skeletal grainstone interbeds with oolite intraclasts (Figure 1b,g). The lower 20 m of this oolitic interval shows occasional dune-scale cross-stratification and contains 3–5 m-wide, 1–2 m-high

archaeocyathan patch reefs from which we took the sample for this study (Figure 1g). Previous authors have documented that these reefs have a much higher archaeocyath abundance (~38% estimated volume) and mostly contain two genera (*Paranacyathus* and *Protopharetra*), with numerous examples of branching visible in the field (Figure 1c; Rowland & Gangloff, 1988). The specimen studied herein is from the irregular archaeocyath genus *Protopharetra*. The fact that these in situ reefs are associated with an oolite indicates that they grew in shallow, wave-agitated waters much like modern coral reefs (Lidz et al., 2006).

In Labrador, archaeocyathan patch reefs are contained within the lower half of the carbonate-dominated Forteau Formation (GPS: 51.47002, -56.83864, WGS84; James & Kobluk, 1978; Pruss et al., 2012). The base of the Forteau Formation is a ~3 m package of dolomitized coarse grainstones, which is overlain by the reef-bearing interval (Figure 1g). The next ~40 m of stratigraphy consists of mostly carbonate mudstone to wackestone beds with abundant patch reefs all less than 1 m in height. The samples we reconstruct from within these reefs contain both dominant genera from the Labrador locality (*Archaeocyathus* and *Metaldetes*). Reefs often have coarse, skeletal grainstone flank beds (Figure 1e,g,h). Toward the top of this reef-bearing interval, oolitic beds become common and archaeocyaths become sparse (Figure 1g).

In the Yukon, large-scale, 50 m-tall × 300 m-wide archaeocyathan reefs are preserved in the Rosella Formation in the Quiet Lake map area of the Pelly Mountains (GPS: 61.526414, -132.314122, WGS84; Read, 1980). The regional stratigraphy has an argillite base with increasing carbonate content upward and several 1–10 m-scale packages of fine-grained limestone with low-angle cross-stratification near the top of the argillite interval (Figure 2c). This predominantly siliciclastic base is overlain by the ~150 m reef-containing unit, within which the reefs may be at least 50 and up to 90 m in stratigraphic height (Figure 2c–e). The reefs contain a diverse assemblage of archaeocyaths, among which, the regular genus *Coscinocyathus* and the irregular genera *Pycnoidocyathus* and *Protopharetra* are the dominant taxa (Read, 1980). In this study, the samples we reconstruct are from the genus *Pycnoidocyathus*. Where reefs are not present in this unit, the laterally equivalent lithology is a nodular limestone with dolomitized burrows and varying levels of argillite and skeletal content (Figure 2c). Overlying the reef-bearing unit is a succession of five sequences, within each of which the nodular limestone facies has upward increasing argillite content before becoming nearly pure argillite (or cover interpreted as argillite; Figure 2c). Given the finely bedded and fine-grained nature of much of the succession, the ambient environment likely was low energy with varying degrees of input from an avulsing siliciclastic source. Coarse-grained skeletal material and ooids in the beds adjacent to the reefs (Figure 2c,e) indicate reef tops were above wave base, so that high-energy perturbations would have interacted with reefal topography.

Both the Nevada and Yukon localities fall within the Montezuman Stage of the Waucoban Series (Laurentian equivalent of the global Series 2), based upon Laurentian trilobite

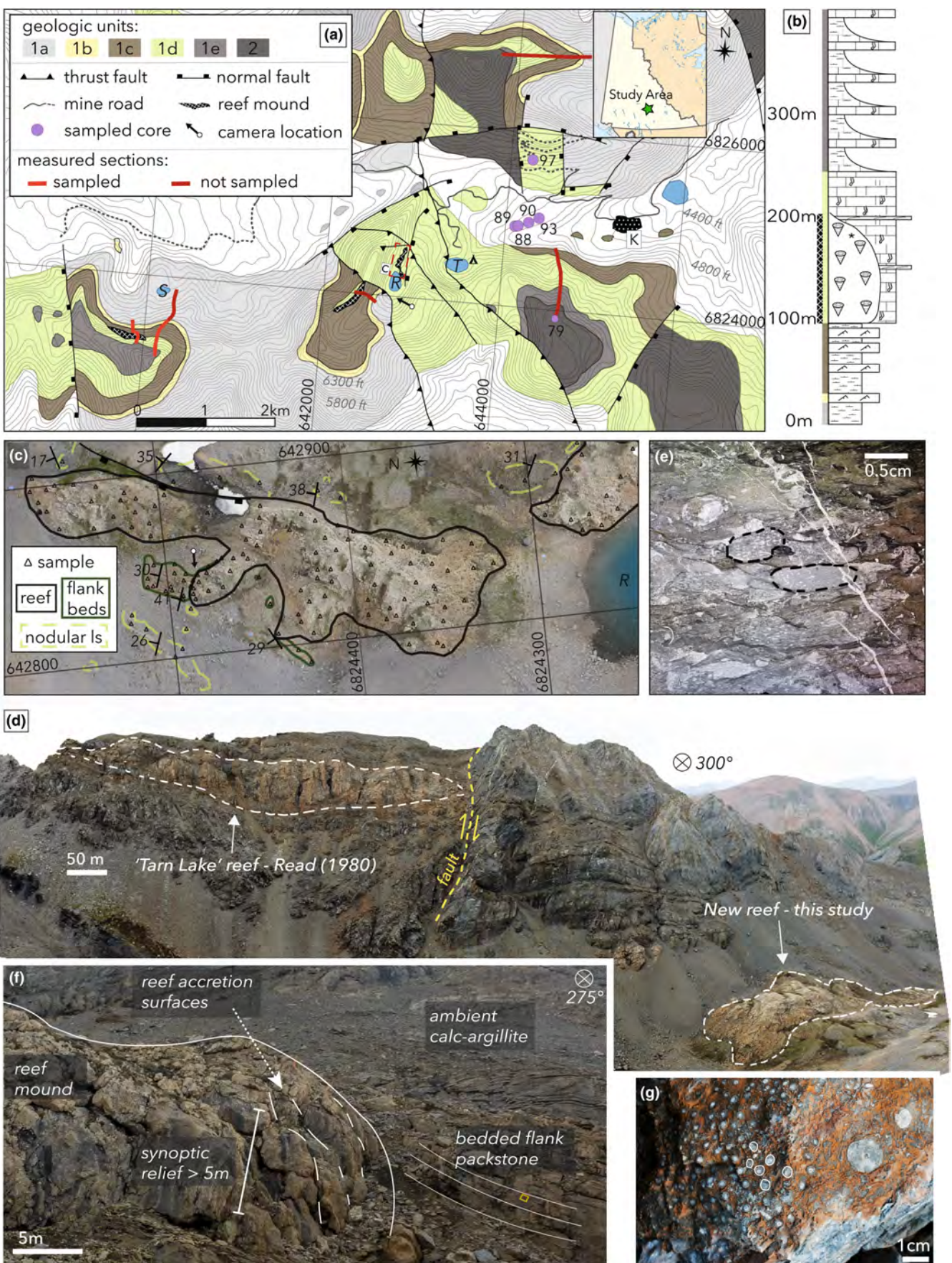


**FIGURE 2** Extended documentation of the Yukon site and the newly discovered reef. (a) Geologic map of the study area, modified from Read (1980). Geologic units are after Read (1980), and correspond to the colored sections of our generalized stratigraphy for the area (b; see Figure 1 for legend and main text for discussion). Uncolored areas are unmapped and/or covered. Dotted mine roads are not passable by standard vehicle. For this study, we logged and sampled existing cores from a previous mining operation at this site, abbreviated on the map with their final two identifying digits. Four of the cores intersect a reef mound at the following depths: KR-11-1588; 209–170 m, KR-11-1589; 194–162 m, KR-11-1590; 137–113 m, KR-11-1593; 94–62 m, indicating another large-sale reef buried near those four bore holes. The intact archaeocyathide sample from this site comes from core KR-88-297. This core and its log mostly had been lost, so a depth could not be determined for this sample. Camera location is for the image in (d). Area labeled with “K” is the remaining Ketza Mine facility, and the tent symbol is our camp site. Contour interval is 100 ft. (c) Drone-derived orthophoto of the newly discovered reef, along with geologic boundaries (all within unit 1d) and sampling locations. Camera location is for the image in (f). All areas not enclosed by polygons are covered. (d) Panoramic image depicting the relationship between the Tarn Lake reef originally documented by Read (1980) and the new reef reported herein. The two reefs shown here, along with all other reefs in the region, come from the same ~150 m-thick stratigraphic interval. (e) Example thin section micrograph of a sample from the new reef locality with traces of irregular archaeocyathides, like those reconstructed in three dimensions in this study. (f) Oblique view of the new reef locality in which adjacent flank beds onlap the mound, and accretionary surfaces indicate the reef maintained at least 5 m of synoptic relief in life. The adjacent reef-flank beds are skeletal and coarse-grained, demonstrating that at least the reef crest was above wave base, unlike the ambient low-energy conditions indicated by the regional prevalence of calc-argillite. (g) Close-up outcrop image of a densely branching archaeocyathide in a partly dolomitized matrix typical of the Yukon site

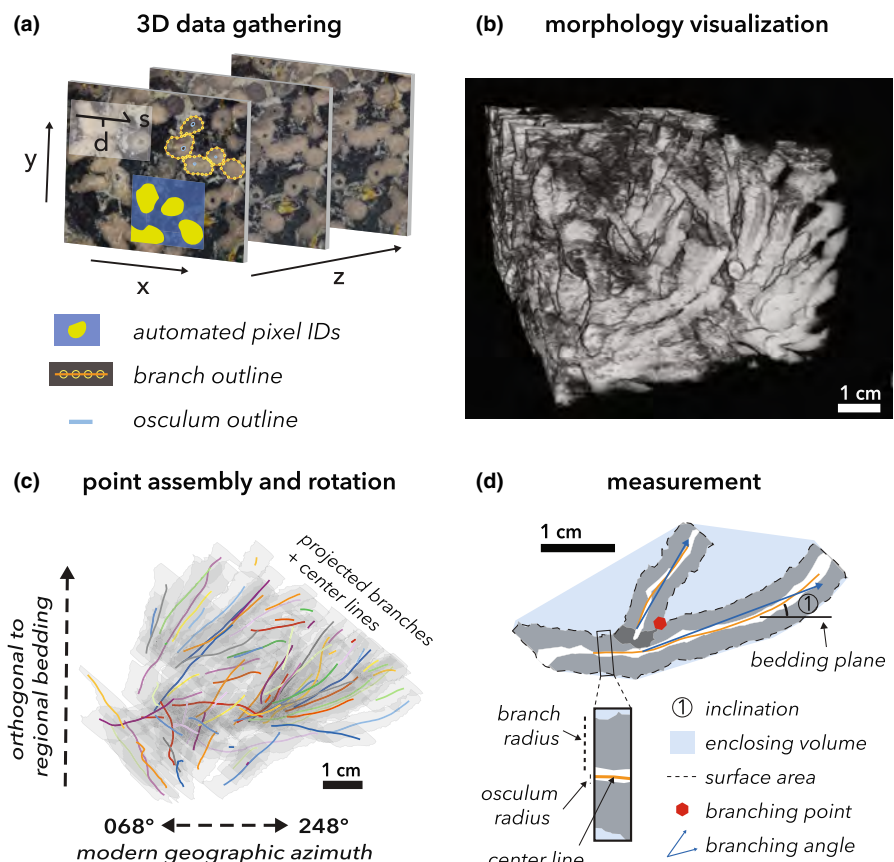


**FIGURE 3** Method for three-dimensional (3D) visualization and measurement of branching archaeocyathides. (a) Serial grinding and imaging of samples produces a 3D voxelated dataset, with x- and y-axes defined by the pixel coordinates (5.2  $\mu\text{m}$  resolution at full scale) in individual image planes and the z-axis defined by the vertical spacing (20  $\mu\text{m}$ ) between grind cycles. Pixels from the automated image segmentation pipeline (a) are stacked into 3D for overall morphology visualization of branching archaeocyathides (b; Figure 4). (c) Skeleton and osculum outlines are assembled into 3D space, guided by the z position of each image. The point clouds defining each archaeocyathide branch are rotated to a tilt-corrected position where the regional bedding plane is horizontal. Depicted here is a two-dimensional (2D) orthographic projection of the outline point cloud (gray) for each branch, as well as the center lines (colored lines). (d) With the 3D center lines, as well as point clouds, metrics of the branching system can be calculated. Again, the fully 3D measurements are illustrated here through 2D projection.

biostratigraphy (Hollingsworth, 2011; Read, 1980). The Labrador reefs are younger, likely occurring in the middle of the Dyeran Stage, also of the Waucoban series (James & Kobluk, 1978). Currently,

there are no radiometric ages to further refine the age differences between the sites or place the Laurentian trilobite stages in absolute time in comparison with other localities globally. The

provinciality of Cambrian faunas, along with the ambiguity of  $\delta^{13}\text{C}$ , Hg, and  $^{87}\text{Sr}/^{86}\text{Sr}$  correlation, limits comparisons of Laurentian sections to global biostratigraphic and chemostratigraphic age models (Dilliard et al., 2007; Faggetter et al., 2019; Montañez et al., 2000; Skovsted et al., 2021; Wotte et al., 2011). However, based upon current age constraints for the base of the Montezuman and the top of the Dyeran Stages—from detrital zircon studies, sedimentation rate modeling, and species duration estimates—the maximum age range for the three samples is 18 million years, and more likely estimates of the age range are 5–10 million years (Karlstrom et al., 2018, 2020; Peng et al., 2020; Sundberg et al., 2020). Notably, the three reefs we study within the Waucoban Series are contemporaneous with the local proliferation of large, skeletonized metazoans (Peng et al., 2020).

## 2.2 | Documentation of new reef at Yukon locality

The Yukon locality originally was mapped by Read (1980) and mentioned in subsequent review studies (Rowland & Gangloff, 1988; Rowland & Shapiro, 2002). However, all previously studied reefs at this site are preserved in steep cliffsides and are not suitable for detailed spatial observation, mapping, and sampling. While performing field work for this study, we discovered a reef on the floor of a glacial cirque, adjacent to the “Tarn Lake” section and reef of Read (1980; Figure 2a,d). The erosion of overlying strata has left over 15,000 m<sup>2</sup> of reef exposed and easily accessible for detailed study.

## 2.3 | Field methods

To produce base maps of the Nevada and Yukon localities, we gathered aerial imagery with a senseFly eBee fixed-wing drone at a resolution under 4 cm per pixel and stitched the drone-derived images into orthomosaics with Agisoft Metashape software. Because the Labrador locality is not as suitable for drone photography, we gathered base imagery with a handheld camera attached to an orientation-tracking tripod. The Labrador images also were stitched into a 3D model and orthomosaic with Agisoft Metashape. We geo-referenced imagery in drone-derived photographs with the corner locations of 1.2 × 1.8 m blue tarps, constrained by multiple observations with a Trimble GeoXH Rover differential GPS (dGPS) unit (<0.2 m uncertainty). Our ground control points for the Labrador imagery were 8 × 13 cm notebooks laid on the outcrop, constrained by multiple dGPS observations. At all three localities, samples and observations were collected by walking an approximate grid with ~10 m spacing. We collected each sample as an oriented block on which we marked the strike and dip of a roughly planar surface on the rock prior to extraction with a hammer and chisel. We marked the location of each sampling point with a dGPS observation and local bedding orientation. This workflow yielded over 160 samples per locality that will be the subject of future chemical and physical

analyses. A selection of larger samples was chosen for 3D analysis in this study.

## 2.4 | 3D morphological measurement and analysis

All samples consist of carbonate fossils surrounded by carbonate sediments and cements, and thus lack the necessary density contrast for 3D morphological analysis through X-ray computed tomography (CT). To analyze the morphology of reef-building archaeocyathides from each of the three field sites, we use the Grinding, Imaging, and Reconstruction Instrument (GIRI; Mehra & Maloof, 2018; Mehra et al., 2020; Howes et al., 2021), which leverages optical contrast to distinguish fossils from their surrounding matrix in three dimensions. Prior to sample grinding and imaging, we record the orientation of the image plane with respect to the field site to allow for later analysis in tilt-corrected coordinate space. In this study, we adopt two separate techniques to process GIRI image stacks (Figure 3). The first technique produces 3D volume renderings for qualitative descriptions of overall morphology, and the second technique produces a 3D point cloud that can be measured and quantitatively compared with other reef-building organisms.

### 2.4.1 | Analysis path a: Gross 3D morphology visualization

Our solution for producing visuals of overall archaeocyathide morphology follows the semi-automated image analysis pipeline of Mehra and Maloof (2018). On approximately five images per sample, we manually trace several instances of archaeocyathide fossils and their surrounding matrix to serve as a training set for a Convolutional Neural Network (CNN). This technique uses stochastic gradient descent to learn the optimal set of feature-detecting filters to distinguish between the two classes in each sample. After training, we apply the network to the entire image stack for a given sample to yield pixel-wise classifications for each image (Figure 3a). The resulting stack of archaeocyathide-identified pixels can be loaded into software for volume rendering and visualization of the overall morphology (Figures 3b, 4a–c). Following this path, we recognize densely branching habits in the archaeocyathide fossils; however, spurious pixel identifications add noise to the model and limit automated and accurate measurement of the branching structure.

### 2.4.2 | Analysis path b: 3D morphological measurements

To obtain the most accurate dataset for 3D measurement of archaeocyathide branching systems, we opt for manual tracing. On a downsampled set of the original images, we trace the outlines of each branch, as well as the oscula, such that each branch can be represented as a set of

2D coordinates in the image plane (**Figure 3a**). We assemble the points defined by the 2D tracings into 3D space, guided by the z position of each image. We then use rotation matrices constrained by the image plane strike and dip, as well as the regional bedding for the field site, to rotate the 3D point clouds defining each branch to a tilt-corrected position. In this coordinate system, where the regional bedding plane is horizontal, we make the following set of measurements:

- **Branching point locations:** We identify the branching points by moving down the z-axis and flagging the points at which the outlines of two branches first overlap or touch (**Figure 3d**).
- **Standardized surface area to enclosing volume ratio (sSA/EV):** To avoid biases stemming from sample size, we measured the surface area of all specimens that fit within a standard-sized cube measuring  $4 \times 4 \times 4$  cm, making that measurement at 100 random points on each model. This standard cube size was chosen as it could be applied to even the smallest archaeocyathide models to give an accurate comparison of roughness. We calculate surface area as the perimeter of all branches in each traced image plane multiplied by the distance between each traced image. If two branch traces overlap in any image plane, we remove the outlines within overlapped regions and use a single outline around the set of branches to calculate the perimeter. The final ratio we report takes the total surface area within the standard cube and is divided by the cube volume.
- **Branch center lines:** To calculate the center line of each branch, we first take the singular value decomposition (SVD) of the branch's point cloud to produce a rotation in which the x-axis represents the long axis of the branch. We then evenly segment the branch along the x-axis and calculate the centroid of all outline points within each segment. The line connecting all centroids then traces the center line, which we rotate back to tilt-corrected coordinates (**Figure 3d**).
- **Branch and oscula radii:** We calculate branch and oscula radii by moving along each branch center line at regular intervals. At each sampling point, we use the derivative of a spline fit to the center line to indicate the local branch heading. We then sample the plane perpendicular to the local heading vector and define the radius of the branch or osculum as the mean distance between all points on that plane and the center line (**Figure 3d**).
- **Branch inclinations:** We calculate branch inclinations simultaneously with branch radii. At each sampling point, we convert the local center line derivative to an inclination (**Figure 3d**) with the equation:

$$\theta_{inc} = \tan^{-1} \left( \frac{dz}{\sqrt{dx^2 + dy^2}} \right)$$

- **Branching angles:** To calculate branching angle, we go to each branching point and identify the points at which the two branch center lines become closest. We take all center line points in each

branch segment past this junction up to the end of the branch or until it has a branching point with an additional branch. The branching angle we calculate is the angle between the mean growth direction of the two segments. For each segment, we calculate unit vectors heading from the junction point to all other points on the center line of the segment. The mean growth direction is the mean of these unit vectors. We calculate the angle between the two mean growth directions ( $\overline{br}_1$  and  $\overline{br}_2$ ) with the following equation:

$$\theta_{br} = \arctan2 \left( \left\| \overline{br}_1 \times \overline{br}_2 \right\|, \overline{br}_1 \cdot \overline{br}_2 \right)$$

- **Branch spacings:** To calculate branch spacings, we take the mean heading of all branches in the specimen and rotate the point cloud such that the mean heading is pointed vertically. We then sample x-y planes at regular intervals along the z-axis and calculate the distance between each branch within the plane and its nearest neighbor. We compute the mean branch spacing of each system by taking the mean of all distances over every sampled plane.

## 2.5 | Analog material for comparison to fossil archaeocyaths

Modern corals and sponges, as well as fossil archaeocyaths, produce a wide variety of gross morphologies. In this study, we specifically concentrate on a comparison between branching forms, because branches often are the site of phenotypic plasticity (Shaish et al., 2007). Here, we define phenotypic plasticity as the effect of the surrounding environment on the phenotype or morphology of the organism within its lifetime, independent of genetic differentiation (Todd, 2008). On the contrary, gross morphological traits often are the result of predetermined genetic characteristics (Shaish et al., 2007). For example, in both corals and sponges, well-developed transport mechanisms within the colony mean that not all polyps or tissues need to be in close contact with moving water carrying organic matter or nutrients, which can lead to the emergence of globular or massive forms (**Figure 5a**; Filatov et al., 2010; Kaandorp, 2013). These morphologies are in contrast with species that have poorly developed transport or aquiferous systems that more often display platey or branching forms (**Figure 5b**; Filatov et al., 2010; Kaandorp, 2013). Because these genetic and soft-tissue underpinnings that lead to the emergence of one gross morphology over another cannot be studied in fossil organisms, we choose instead to study archaeocyathide branching morphologies, which can be compared with modern corals and sponges regardless of genetics and most often display environmental influence (Todd, 2008).

In our initial reconstructions of fossil archaeocyathides, we note dense arrays of narrowly angled and regularly spaced branches (**Figure 4a–c**). These morphological traits are in contrast to most of the known branching morphologies in modern corals and sponges:

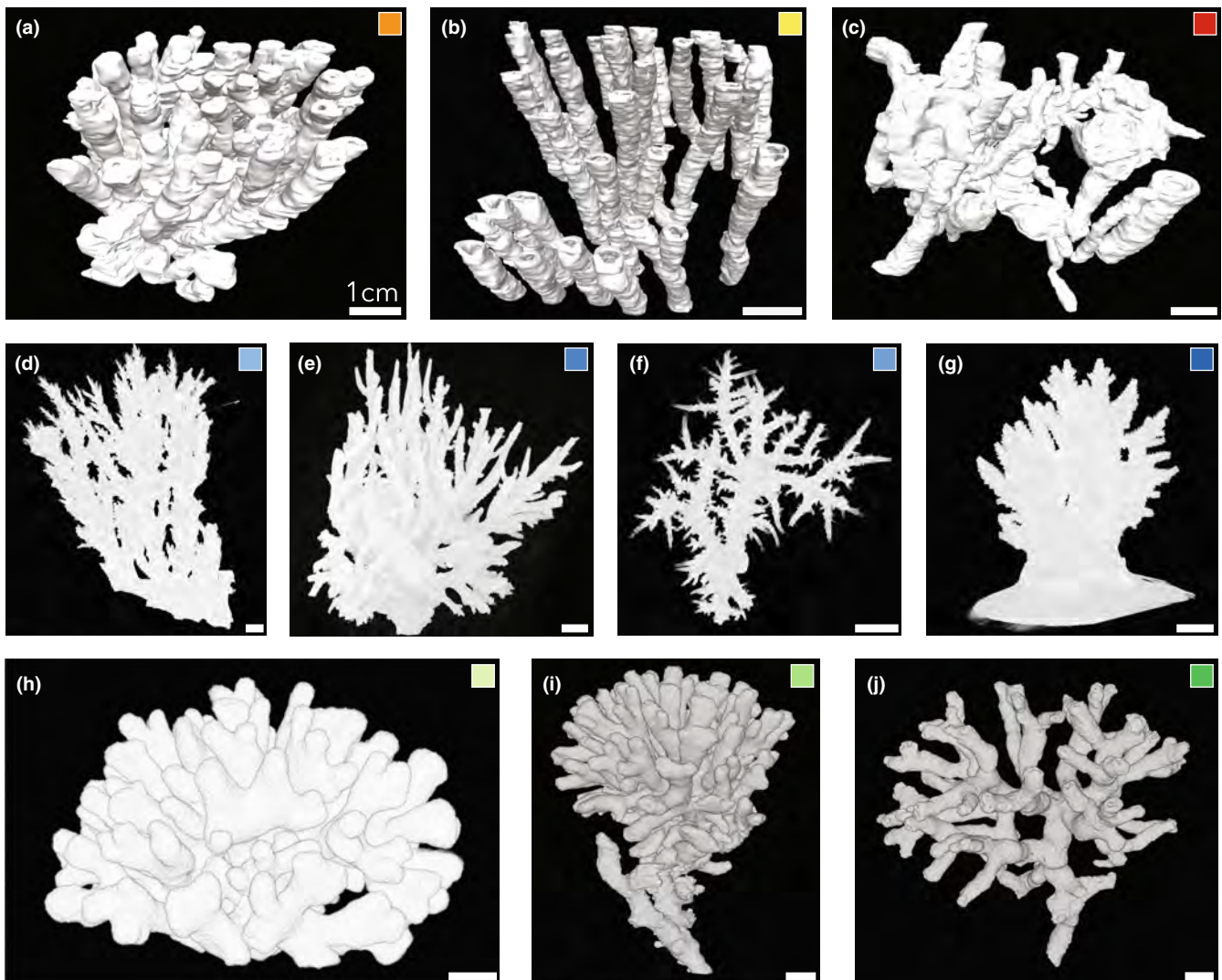
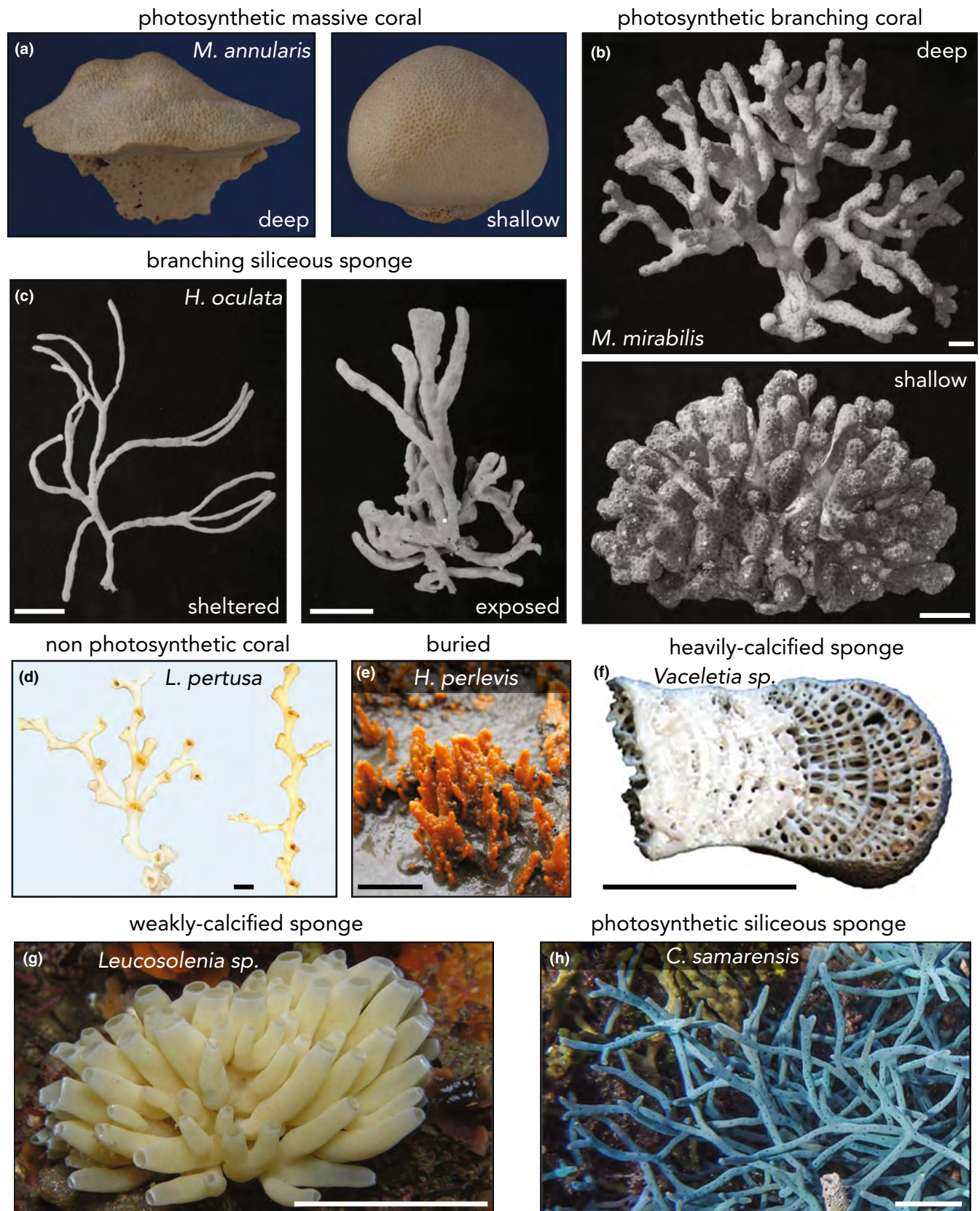


**FIGURE 4** Volume renderings of all archaeocyathide and coral specimens from this study. (a) Nevada archaeocyathide. (b) Yukon archaeocyathide. (c) Labrador archaeocyathide. (d) *Acropora caroliniana*. (e) *Acropora cytherea*. (f) *Acropora loripes*. (g) *Acropora millepora*. (h) *Madracis mirabilis*—6 m depth. (i) *Madracis mirabilis*—15 m depth. (j) *Madracis mirabilis*—20 m depth. Colored squares match the color schemes for samples in Figures 6 and 8.

**FIGURE 5** Brief survey of qualitative morphological characteristics of corals and sponges with varying life modes. (a) *Montastrea annularis* is a massive or globular photosynthetic coral that shows phenotypic plasticity, in that it takes a more platy morphology at depth to better allow polyps to gather attenuated light. Because *M. annularis* has well-connected polyps, its range of phenotypes does not include dense branching networks like *Madracis mirabilis* (b). When polyps are poorly connected, corals like *M. mirabilis* often produce branched networks that show environmental influence in measurable parameters such as branching angle and branch spacing. (c) Dense branching is known in some modern siliceous sponges, such as *Haliclona oculata*. Like corals, these sponges display phenotypic plasticity in their branch thicknesses and spacing that reflect the growth environment. Because the growth of these sponges is not influenced by light as a primary anisotropy, they do not produce regularly spaced, unidirectional branched networks like corals and archaeocyathides. (d) *Lophelia pertusa* is a non-photosynthetic coral that creates fans of widely angled branches with irregular spacings in the absence of light sensitivity. (e) *Hymeniacidon perlevis* is an often-buried sponge that produces irregularly shaped and spaced branches. (f) *Vaceletia* sp. is one of the few known heavily calcified sponges in modern oceans. These often-cryptic sponges do not pair with photosymbionts and therefore are slow-growing and do not produce densely branched networks. (g) Branching is known in modern, calcareous sponges like *Leucosolenia* sp. These sponges also do not pair with photosymbionts and unlike archaeocyathides, remain weakly calcified, flexible, and small. (h) Some siliceous sponges, like *Callyspongia samarensis* do pair with photosymbionts. Because these sponges do not grow through accretionary growth, but instead through interlocking of skeletal elements, their branching morphologies are more a reflection of their underlying skeletal architecture and do not form a good point of comparison for archaeocyathides. Scale bars are 1 cm.



- **Fully-encrusted and buried sponges:** Some modern sponges develop branched habits while mostly buried or encrusted (e.g., Clionaidae, *Hymeniacidon perlevis*; [Figure 5e](#)). As very little of the organism is influenced by the water column, these sponges develop highly irregular branches, both in terms of shape and spacing (Erpenbeck & van Soest, [2002](#)).
- **Densely-branching, siliceous sponges (non-photosynthetic):** Somewhat-dense branching arrays can arise in sponges that have a poorly developed aquiferous system (e.g., *Haliclona oculata*; [Figure 5c](#)). Because more of the colony must be in contact with the surrounding water to compensate for weak circulation within the organism, these sponges have thin, delicate branches, especially in calm environments (Kaandorp et al., [2005](#)). In higher-energy environments, these sponges can develop asymmetrical fan or paddle shapes perpendicular to the flow. In all environments, these sponges show irregular, sometimes wide, branch spacing (Kaandorp et al., [2005](#)).
- **Branching, photosynthetic, siliceous sponges:** Some siliceous sponges do pair with photosymbionts (e.g., *Callyspongia samarensis*; [Figure 5h](#)). There is currently no evidence that growth direction of these sponges is heavily influenced by light sensitivity, like calcitic corals. Because taxa-like *Callyspongia* do not grow through accretionary growth, but instead through interlocking of skeletal elements, their branching morphologies are more a reflection of their underlying skeletal architecture (Erpenbeck et al., [2012](#)).
- **Densely-branching, calcareous sponges (non-photosynthetic):** Dense branching arrays also develop in some calcareous sponges (e.g., *Leucosolenia*; [Figure 5g](#); Erpenbeck & van Soest, [2002](#)). However, these animals are weakly calcified and their branches remain flexible, unlike the heavily calcified branches of archaeocyathides.
- **Heavilycalcified sponges:** Although some sponges do display heavy calcification (e.g., *Vaceletia*; [Figure 5f](#); Vacelet, [2002](#)), they are rare, often-cryptic, and deep-water animals. There are no examples of a shallow-water, heavily calcifying sponge that produces a densely branched network. Because these sponges do not associate with photosymbionts, it likely is not energetically possible for them to rapidly accrete carbonate in the shallow benthos in a way that would lead to branching (Goreau, [1959](#)).
- **Non-photosynthetic corals:** Non-photosynthetic corals (e.g., the deep-water scleractinian *Lophelia pertusa*; [Figure 5d](#)) have wide-angled branch arrays (Sanna & Freiwald, [2021](#)), where the growth is impacted by the predominant current or flow, and irregular, fan-like colonies are formed (Kaandorp, [1999](#)).

### 2.5.1 | Photosynthetic corals

Examples of symmetrically-spaced, narrow-angled branches today most commonly are known from scleractinian corals that host photosymbionts ([Figure 5b](#); Filatov et al., [2010](#); Kaandorp, [2013](#);

Todd, [2008](#)). The regularity in branch spacing in photosymbiotic corals comes from the need to flush photosynthetic waste products from the interior of the colony, as well as growth that is sensitive to light, which produces radial symmetry (Filatov et al., [2010](#); Todd, [2008](#)). The anisotropy in growth direction also leads to narrower branching angles and less variance in branch heading ([Figure 6](#); Filatov et al., [2010](#); Kaandorp, [2013](#)). Given that the branching characteristics we recognize in our archaeocyathide specimens today are otherwise found only in photosynthetic corals, they form the most logical point of comparison for our quantitative study. Although 3D morphological data for many of the forms outside of photosynthetic corals surveyed above do not exist, their physiologies and qualitative morphologies indicate that their life modes and measurements would be different from those of archaeocyathides.

As the first analogy between branching archaeocyathids and modern photosynthetic corals, we used our measurement pipeline on synthetic models created through accretionary growth simulations from Filatov et al. ([2013](#)). These models give a baseline for branching measurements typical of accretionary growth systems, like archaeocyaths and corals, and provide insight on how those metrics change under different environmental conditions. Namely, the model set from Filatov et al. ([2013](#)) explore how light sensitivity in accretion alters branching forms, allowing us to see the influence of photosymbiosis on branching measurements. Details on the synthetic modeling process can be found in Filatov et al. ([2013](#)).

We also used our pipeline to measure X-ray computed tomography (CT) scans of seven branching scleractinian corals. Four of the specimens are of the genus *Acropora* from the collections of the Field Museum of Natural History ([Figure 4d-g](#); *A. millepora*—FMNH I 15962; *A. loripes*—FMNH I 15959; *A. caroliniana*—FMNH I 15953; *A. cytherea*—FMNH I 245). The other three coral specimens are of the species *Madracis mirabilis*, collected on a depth transect along the Curaçao reef and previously studied by Kruszyński et al. ([2007](#); [Figure 4h-j](#)). In the case of both the synthetic accretionary growth models and coral CT scans, the voxelated 3D datasets had adequate contrast between the specimen and its surroundings such that we could write an algorithm to trace the branches automatically.

To compare the substrate geometry of archaeocyathan reefs to microbial reefs of the Precambrian, we developed synthetic models of stromatolites, from which we could measure surface area and roughness. We chose synthetic models to represent microbial reefs because 3D data from fossil or extant stromatolites of diverse morphologies are lacking. To model stromatolites, we started with the compilation of carbonate stratigraphic columns of Cantine et al. ([2020](#)), and extracted all strata with a reported stromatolite occurrence within each time bin in the database. We created point cloud models of the four predominant stromatolite forms reported (low domal, columnar/digitate, conical, and giant) with morphologies based upon Walter ([1976](#)). We specifically modeled versions of each morphology where multiple stromatolites grow together

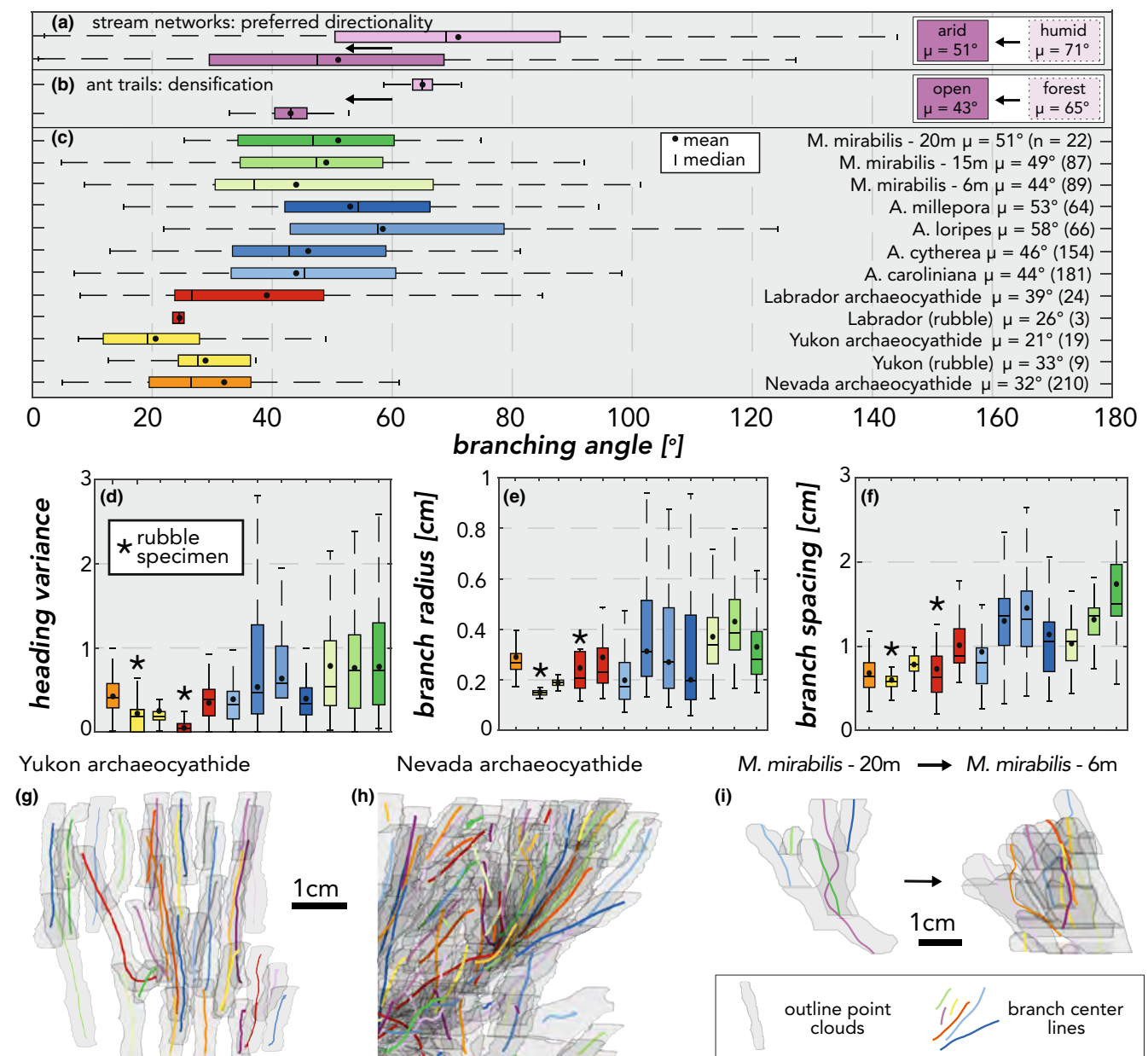


**FIGURE 6** Emergent branching systems and their morphological interpretations. (a) Arid, high-relief environments are an example of a setting where the overall channel system shares a common slope and preferred directionality, leading to relatively narrow branching angles between streams, compared with low-relief, humid environments (Getraer & Maloof, 2021). (b) In open environments without falling debris, the benefits of shorter overall paths outweigh the material cost of having to maintain a denser array of paths for leaf-cutting ant colonies, creating narrower angles within the network (Farji-Brener et al., 2015). (c) Both modern reef-building corals and Cambrian reef-building archaeocyathides have narrow branching angles, implying that both systems are more heavily influenced by preferred directionality as opposed to material cost or energetic limitation, and benefit from a dense array of branches. The *Madracis mirabilis* specimens have an increasing mean branch angle with increasing depth, reflecting the need to maintain a more open framework in lower-energy waters (Kruszyński et al., 2007). Compared with modern corals, archaeocyathide specimens maintain a more uniform growth direction (d), more consistent branch radii (e), and smaller branch spacings (f). In addition to intact framework archaeocyathide specimens from each locality, we include morphological data from rubble specimens (\*) that still preserve examples of branching. In all box and whisker plots, whiskers span the 5–95 percentiles, and boxes span the 25–75 percentiles. (g–i) Example orthographic projections of 3D archaeocyathides and corals illustrate concepts from d–e

and coalesce to more accurately represent the substrate geometry of Precambrian reefs. To get the mean roughness of stromatolite reefs within each time bin, we took the mean sSA/EV of all

occurring forms, weighted by the thicknesses of the strata within which they occur. This approach approximates the influence of overall synoptic relief and gives a maximal estimate of stromatolite

TABLE 1 3D measurements from archaeocyathide specimens and modern reef-building *Madracis* and *Acropora* (A.) corals

Specimen	Mean branch angle [°]	Mean branch radius [cm]	Mean branch spacing [cm]	Mean osculum radius [cm]	Mean sSA/EV [ $\text{cm}^{-1}$ ]	Mean branch heading variance
Nevada archaeocyathid	$32 \pm 21$	$0.29 \pm 0.08$	$0.68 \pm 0.25$	$0.063 \pm 0.030$	$0.93 \pm 0.23$	0.42
Yukon archaeocyathid	$21 \pm 12$	$0.19 \pm 0.03$	$0.62 \pm 0.16$	$0.081 \pm 0.008$	$1.09 \pm 0.04$	0.24
Labrador archaeocyathid	$39 \pm 25$	$0.29 \pm 0.11$	$1.04 \pm 0.48$	$0.048 \pm 0.001$	$0.44 \pm 0.17$	0.35
Yukon rubble	$33 \pm 18$	$0.15 \pm 0.05$	$0.74 \pm 0.22$	$0.077 \pm 0.017$	NA	0.23
Labrador rubble	$26 \pm 2.1$	$0.25 \pm 0.08$	$0.82 \pm 0.24$	$0.085 \pm 0.060$	NA	0.12
<i>Madracis</i> 6 m—shallow	$44 \pm 25$	$0.30 \pm 0.16$	$1.06 \pm 0.27$	NA	$1.58 \pm 0.26$	0.89
<i>Madracis</i> 15 m	$49 \pm 23$	$0.43 \pm 0.16$	$1.35 \pm 0.25$	NA	$0.81 \pm 0.48$	0.77
<i>Madracis</i> 20 m—deep	$51 \pm 24$	$0.33 \pm 0.16$	$1.78 \pm 0.67$	NA	$0.5 \pm 0.17$	0.86
<i>A. caroliniana</i>	$44 \pm 18$	$0.22 \pm 0.13$	$0.96 \pm 0.26$	NA	$0.72 \pm 0.24$	0.38
<i>A. cytherea</i>	$46 \pm 20$	$0.31 \pm 0.26$	$1.43 \pm 0.61$	NA	$0.4 \pm 0.27$	0.48
<i>A. loripes</i>	$58 \pm 22$	$0.27 \pm 0.23$	$1.49 \pm 0.46$	NA	$0.33 \pm 0.18$	0.59
<i>A. millepora</i>	$53 \pm 18$	$0.20 \pm 0.21$	$1.17 \pm 0.39$	NA	$0.86 \pm 0.14$	0.40

Notes: The rubble specimens for Yukon and Labrador localities are not intact branching frameworks like the other three fossil specimens but are instead preserved branching examples found within fossiliferous rubble samples. Numbers following  $\pm$  are one standard deviation. sSA/EV stands for standardized Surface Area/Enclosing Volume.

reef roughness, assuming the entire reef remained unburied by interstitial sediments.

### 3 | RESULTS

Results are reported in Table 1. The branching metrics we measure, such as angle and spacing, serve as proxies for the local current or wave energy in the growth environment, as well as the physiology of the animals themselves. The full set of coral specimens studied has a relatively narrow mean branching angle of  $50^\circ$ . In archaeocyathide fossils, we see an even narrower distribution of branching angles with a mean of  $31^\circ$ . In the depth transect of *Madracis mirabilis* specimens, there is a narrowing of mean branching angle going from the deepest specimen to the shallowest (Figure 7c), which also is accompanied by a decrease in branch spacing (Figure 7f). The shallowest *Madracis* morph also exhibits the most regularity in branch spacing (Figure 7f). The archaeocyathide specimens have more regular branch radii than the coral specimens and maintain smaller branch spacing (Figure 7e,f).

Our sSA/EV measurements serve as a proxy for how much active area can interact with a given parcel of water to perform nutrient exchange and waste ejection—often termed mass transfer (Figure 8; Lowe, Koseff, & Monismith, 2005; Lowe, Koseff, Monismith, & Falter, 2005; Monismith, 2007; Reidenbach et al., 2006). The Nevada and Yukon archaeocyathide specimens exhibit surfaces with mass transfer potentials only exceeded by the shallowest *Madracis* morph (Figure 8). Even the lowest archaeocyathide sSA/EV measurement seen in the Labrador specimen is comparable to several of the analyzed *Acropora* species. The archaeocyathides analyzed here fill a given volume with just as much or more surface area as corals building diverse reefs in the Recent (Figure 8).

### 4 | DISCUSSION

#### 4.1 | The interpretation of branching morphologies

Branching systems are ubiquitous in nature; from blood vessels, to ant trails, to stream networks, natural systems produce many forms and scales of branched organization (Figure 6a). Here, we are concerned with a particular class of system, whereby branching arises strictly through diffusion limitation, as opposed to genetic signaling or other mechanisms. Because these systems are the result of physical or chemical gradients that promote propagation in the direction of the most rapid change in surface slope (Kaandorp et al., 2005; Petroff et al., 2011), their morphologies provide a proxy for characteristics of the growth environment. With local surface curvature as the basis of propagation, the morphology of a system can be seen as the result of an optimization process to respond to anisotropies in the growth environment and to reduce costs (Roy, 1983; Roy & Woldenberg, 1982). Environmental anisotropy gives a preferred growth direction to all branches, therefore narrowing branching angles (Figure 7a; Getraer & Maloof, 2021; Sagy et al., 2001). The energetic or material costs of maintaining each branch dictate the number and thickness of branches in the system, where a higher density again leads to narrower angles (Figure 7b; Farji-Brener et al., 2015).

In the case of skeletal accretionary growth in corals and archaeocyathides, the primary cost-benefit optimization relates to the energetically expensive process of precipitating calcium carbonate (Kaandorp et al., 2005). To enhance carbonate precipitation, densely branching corals pair with zooxanthellate photosymbionts that contribute metabolic energy to the system (Al-Horani et al., 2003) and locally drive up the carbonate saturation state (Al-Horani et al., 2003; Geyman & Maloof, 2019). Photosymbiosis introduces an anisotropy from light sensitivity to coral accretion, which drives

branches to grow toward the light (Muko et al., 2000; Todd, 2008), leading to forms with narrower branching angles and less variance in branch growth direction—results borne out in both synthetic branching experiments (Figure 6b,c; Filatov et al., 2010) and field observations (Muko et al., 2000; Todd, 2008).

The morphological consequences of photosymbiosis also are manifest in branch spacing. In all environments, branching is an emergent process, whereby the resulting branch spacing must be wide enough to avoid stagnant zones within the colony for efficient flushing of photosynthetic waste products and mass transfer (Monismith, 2007; Reidenbach et al., 2006), while keeping the colony robust to avoid breakage. In the case of oscillatory flow regimes, which commonly exist over reef environments, branch spacing in coral colonies can be aligned with the frequency of the wave orbitals such that flow is amplified within the colony, producing fluid velocities equal to or greater than the adjacent free stream (Monismith, 2007; Reidenbach et al., 2006). Photosynthetic corals in higher-energy flow regimes tend to have a denser array of more narrowly angled branches and a smaller branch spacing to radius ratio than those in lower-energy environments, as seen in the depth transect specimens of *Madracis mirabilis* (Figure 7). These regularly spaced branching morphologies are in contrast to branching non-photosynthetic corals and sponges that produce fan-like morphologies with little symmetry or regularity in branch spacings in the face of flow direction as the primary environmental anisotropy (Figure 5d,h; Kaandorp, 1999).

## 4.2 | Implications of archaeocyathide branching measurements

Previous workers have presented data indicative of prey partitioning among archaeocyaths, which reduces competition between reef builders and is a strategy seen in modern corals (Antcliffe et al., 2019). Our results add efficient suspension feeding in oscillatory flow regimes and the harboring of photosymbionts as further convergent adaptations displayed by archaeocyathides and modern corals. The archaeocyathide specimens show the same or even greater regularity in branch spacing compared with shallow-water corals (Figure 7f), indicating growth in energetic, oscillatory environments. The inferred physiology of archaeocyaths as sponges (Rowland, 2001) provides a reduced-cost explanation for densification and can explain the narrower angles and smaller branch spacings seen in comparison with corals (Figure 7c,f). Archaeocyaths would promote either passive or active pumping (Wood et al., 1992) of water into branches and out of the osculum. Thus, in a given flow regime, archaeocyathide growth could produce a denser array of branches than a coral, while still avoiding severe flow dampening at the colony's interior (Kaandorp & Kübler, 2001). The relatively low variability in archaeocyathide branching radii (Figure 7e) might imply that the need for water to pump into each branch constrains thicknesses to a narrow set of hydrodynamically favorable values (Asadzadeh et al., 2020).

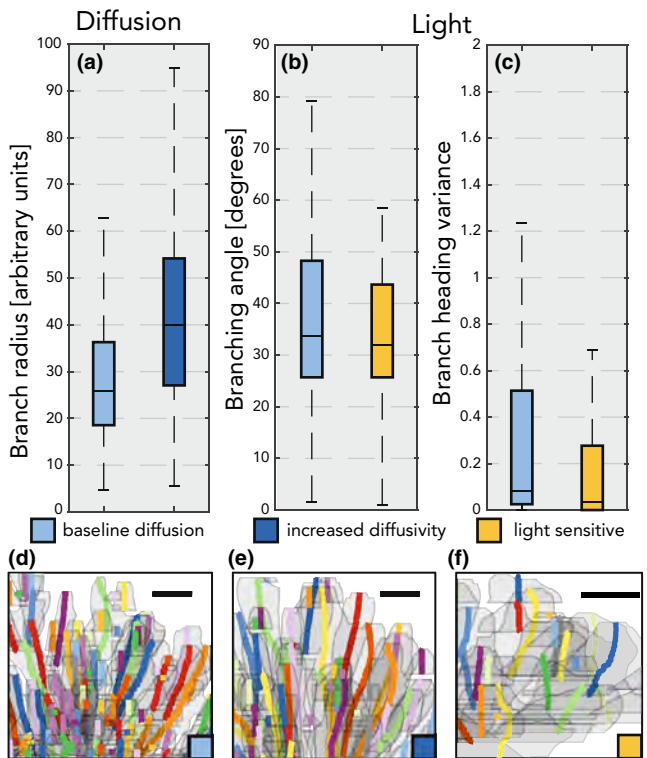


**FIGURE 7** Results of morphological analysis of synthetic accretionary growth experiments. (a) When diffusivity is increased in the system (equivalent to increasing the relative influence of advection), bifurcations become less common and branches become thicker. (b, c) When light sensitivity (modeling the presence of photosymbionts) is introduced as an anisotropy in an accretionary growth system, branching angles become narrower, and the heading of all branches becomes less-variable. (d–f) Example orthographic projections of the measured synthetic-growth models

The association of archaeocyaths with photosymbionts still is debated (Debrenne, 2007). Previous studies investigating the internal cavity morphology of archaeocyaths and the fossil record of dinoflagellates argue against photosymbiosis in the Cambrian (Debrenne & Zhuravlev, 1992; Wood, 1993, 1995), while evidence for external soft tissues (Cowan & James, 1993), carbon isotopes of archaeocyathan reef carbonates (Surge et al., 1997), and occurrences of archaeocyathan reefs in oligotrophic environments (Rowland & Shapiro, 2002) support the presence of photosymbionts. Here, our observations of very narrow branching angles with means near 30°, and consistent branch headings (Figure 7g), imply strongly directional growth. Uniform growth direction, paired with symmetry in branch spacing, are diagnostic morphological traits of branching accretionary growth systems, only known to occur in corals when accommodating the light needs of photosymbionts (Figure 6; Kaandorp et al., 2005; Filatov et al., 2010). Thus, our measurements and quantitative morphological comparisons support the interpretation of branching archaeocyathides as photosynthetically-mediated calcification systems, much like modern corals.

### 4.3 | The available active area of a reef

This convergence of form between archaeocyathides and corals indicates that heightened mass transfer potential due to surface roughness seen on modern coral reefs may have applied to archaeocyathan reef environments. Increased reef roughness—as shown by the high sSA/EV ratios in our archaeocyathide measurements (Figure 8)—was a new feature in Cambrian tropical sea floors compared with the previous 100–300 million years of metazoan evolution.

Sponges originated perhaps hundreds of millions of years prior to archaeocyaths (Brain et al., 2012; Love et al., 2009; Love & Summons, 2015; Maloof et al., 2010; Reitner & Wörheide, 2002; Sperling et al., 2010; Turner, 2021, but see Antcliffe et al., 2014; Bobrovskiy et al., 2021; Botting & Muir, 2018; Zhuravlev, 2015), and other organisms of the Ediacaran biota seem to have expanded upon suspension feeding life modes to couple the benthic and pelagic realms (Cracknell et al., 2021; Droser & Gehling, 2015; Laflamme et al., 2013; Yuan et al., 2011). However, throughout this evolution of putative metazoans, an environment resembling a coral reef—built by large, calcifying suspension feeding organisms—did not exist, and while suspension feeders in the terminal Ediacaran Nama

Assemblage (549–539 Ma), especially *Cloudina* and *Namacalathus*, have been found in and around large microbial boundstones (Penny et al., 2014; Watters & Grotzinger, 2001; Wood & Curtis, 2015), 3D data show that these putative animals were weakly calcified and incapable of reef construction in high-energy flow regimes (Mehra & Maloof, 2018; Schiffbauer et al., 2020). Furthermore, nearly all of the shallow-water Ediacaran suspension feeding organisms were small, often peaking less than a centimeter above the adjacent sediment, and therefore were not a major source of flow-altering relief (Thomas & Atkinson, 1997). During this period, reefs were composed of coalesced stromatolites and thrombolites, which were the primary source of topographic complexity on the seafloor for the first ~3 billion years of life's evolution on Earth. In our coarse record of topographic complexity in Precambrian stromatolitic reefs after Walter (1976) and Cantine et al. (2020), we find that a seafloor built by stromatolites rarely exceeded  $0.2 \text{ cm}^{-1}$  in sSA/EV; most often an order of magnitude lower than archaeocyathide sSA/EV (Figure 8).

Archaeocyathan reefs represent a stepwise increase in the roughness of the seafloor during the early Cambrian, which we term the “Reef Roughness Revolution” (Figure 8). Only once archaeocyathides arose did large, heavily-calcified suspension feeding

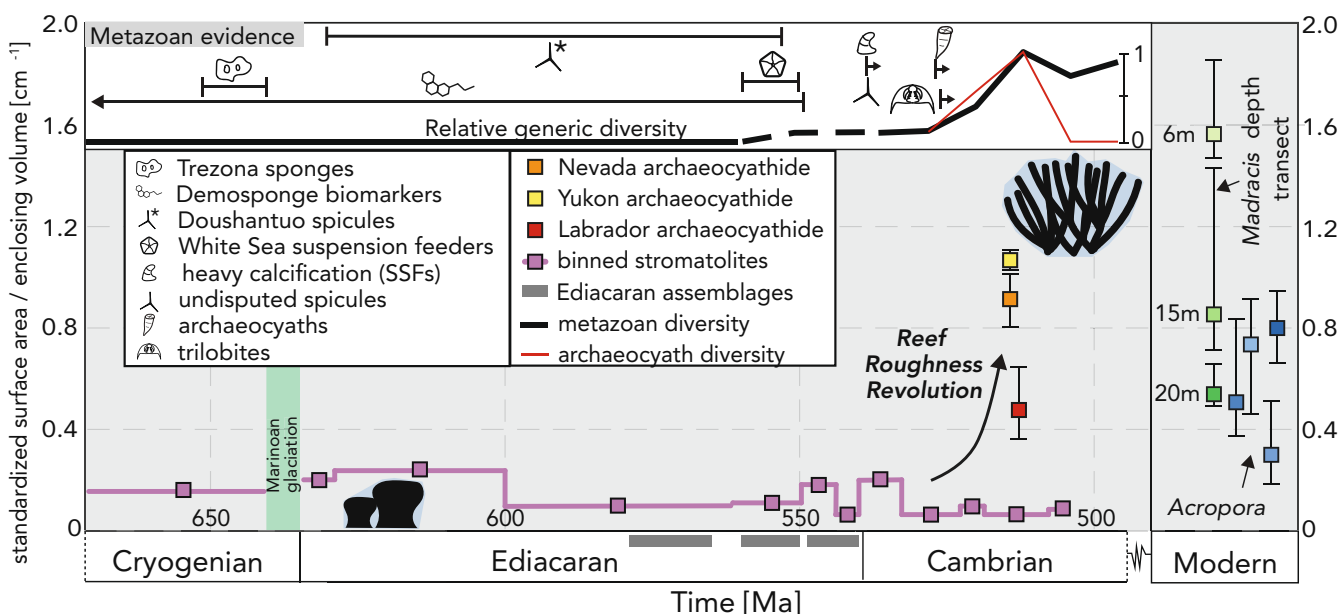


**FIGURE 8** Reef Roughness Revolution. Prior to the rise of archaeocyathan reefs, topography on the seafloor mainly was built by stromatolites (or, to a limited extent, sandy shoals). We modeled several coalesced morphologies of potential reef-building stromatolites (from idealized forms and dimensions after Walter [1976]) and calculated a weighted mean of surface area/enclosing volume (sSA/EV) for each time bin based upon the proportional thickness of each morphology as reported by Cantine et al. (2020). Although proportional thickness does not necessarily scale with sSA/EV, the thickest-bedded stromatolite intervals are most likely to have relatively higher synoptic relief. This stromatolite curve rarely exceeds a value of  $0.2 \text{ cm}^{-1}$ , even in intervals with many occurrences of branched and columnar stromatolites, implying that regardless of stromatolite morphology and thickness, high sSA/EV values are not likely. Our archaeocyathide specimens, all exceed a ratio of  $0.5 \text{ cm}^{-1}$ . The Yukon and Nevada specimens show two of the highest ratios, exceeding all coral specimens except for the shallowest Madracis morphs (points shown are the mean measurement of a  $64 \text{ cm}^3$  cubic volume randomly placed and measured 100 times. Note that we only include archaeocyathide specimens that show a complete, intact branching framework when assessing sSA/EV, as fragmentary specimens do not have enough material to give reliable results for this measurement. Error bars are the 25th and 75th percentiles). Black metazoan diversity curve does not include archaeocyaths; data from the Paleobiology database, accessed August 9, 2021

organisms engineer ecosystems with surface roughness—and therefore mass transfer potentials—similar to modern coral reefs. The establishment of rough reef environments and photosymbiosis would have induced a higher flux of organic matter to the benthos, where deposit feeders and detritivores could become more abundant in and around the reef (Levinton, 1972). Furthermore, a larger trophic base increases the possibilities for higher trophic levels, and thus predation (Griffiths et al., 2017), yielding the net possibility of more complex food webs and inter-animal interactions in the early Cambrian.

The correlation between the rise of archaeocyathan reefs and the proliferation of large, skeletonized taxa like trilobites (Figure 8) does not necessarily imply causation, but their coincidence is provocative. The increase in animal diversity and disparity seen in Cambrian Series 2 and afterward presumably both generated and exploited a broadening range of environments and ecological niches (Marshall & Valentine, 2010; Valentine, 1995). The morphological data we present herein indicate that the added environmental and trophic complexity furnished by the rise of framework reefs and attendant environments should have been a novel ecological driver during the Cambrian radiation.

Because our analysis supports the idea that archaeocyathans built structures—sometimes hundreds of meters long and tens of meters high—that looked and functioned like coral reefs, the question remains as to why fossil occurrence data suggest a paucity of metazoan diversity in Cambrian reefs (Cordie et al., 2019; Rowland & Shapiro, 2002). We consider two scenarios: [1] archaeocyathan reefs were important ecosystems for early animals, but studying their ecology through counts of skeletal remains underestimates the true biodiversity of reefal communities by discounting the contributions of unpreserved animals, or those that did not live within reefs but whose life cycles depended upon reefs (Cordie et al., 2019; Hubbard et al., 1990, 2001; Wood, 1999); or [2] archaeocyathan reefs hosted photosymbionts and looked structurally like modern coral reefs but did not serve as biodiverse habitats, with reefs not becoming centers of diversity until the Ordovician (Cordie et al., 2019). Scenario 1 would indicate that the small-scale geometry of the seafloor is a contributing factor toward trends in marine biodiversity, dating back to the Cambrian radiation (Kiessling et al., 2010). In contrast, scenario 2 suggests that chemical and trophic consequences of rough reef mounds built by branching organisms are not the sole factors that support (and perhaps induce) benthic biodiversity in reefs. We cannot distinguish between these two scenarios yet, but either possibility has important implications for deciphering the cause of the Cambrian radiation. We are hopeful that increasing the number and detail of paleoecological studies on ancient reefs, and quantifying the similarities and differences between reef environments and attendant biodiversity in the early Cambrian versus the rest of the Phanerozoic, will be able to rule out one of these hypotheses.

Ultimately, the convergence of form between Earth's first and current reef builders suggests that selection pressures exist that drive calcified suspension feeding organisms to build rough mounds

with branching forms and associated photosymbionts. Throughout the Phanerozoic eon, the role of reef-builder has been filled by at least one group of animals (Kiessling & Flügel, 2002), providing the aforementioned unique habitats to the contemporaneous biota and potentially serving as preferential sites of speciation (Kiessling et al., 2010). The association between animals and symbionts to create photosynthetically-mediated heavy calcification systems that result in reef mounds may be another important dynamic of our planet that has nurtured the evolution of complex life.

## ACKNOWLEDGMENTS

We thank Kurt Konhauser and James Schiffbauer for editorial handling, and three anonymous reviewers for constructive comments that improved the manuscript. We also thank Akshay Mehra for the help and advice in method development. We are grateful to Emily Geyman, Cedric Hagen, Michael LaBarbera, John Moore, Susannah Porter, Sara Pruss, Peter Tierney, and SITU Studio for useful comments on early drafts and helpful discussions. Alec Getraer provided useful insights on the interpretation of branching angles. We also thank Indu Panigrahi and Nishant Kumar Singhal for their help in developing the image tracing pipelines. We are grateful to Jochen Gerber, Justin Lemberg, Neil Shubin, and the Luo Lab at the University of Chicago for helping to secure CT scans of *Acropora* specimens. We thank Nick Swanson-Hysell for his help with field site paleogeography. Sarah Ward, Sarah Brown, and Akshay Mehra helped conduct field work in Nevada. Bolton Howes, Emily Geyman, and Galen Cadley helped with field work in Yukon Territories. Melvin Rissanen and the team at Boreal Engineering offered generous support for the Yukon field work. Justin Strauss helped in identifying the Yukon field site. Akshay Mehra, Pingping Zhao, Susannah Porter, John Moore, Enrique del Castillo, Jahan Ramezani, and Kaori Tsukui helped in performing field work in Labrador. Funding for this project came from National Science Foundation grants 1410317 and 1028768 to A.C.M., and 1410503 to M.W., as well as the Tuttle Invertebrate Fund and the Geoscience Student Research Fund at Princeton University.

## CONFLICT OF INTEREST

The authors declare no competing interests.

## DATA AVAILABILITY STATEMENT

All data presented in this manuscript are stored permanently on Princeton DataSpace (DOI <https://doi.org/10.34770/rstc-eq70>). This repository includes downsampled versions of three-dimensional image data used in this study, which are adequate to reproduce our results. Full-resolution (>2 Tb) image stacks are available upon request, as explained in the README file in the repository.

## CODE AVAILABILITY

All codes for measurement and data analysis are included in this public repository. [https://github.com/rmanzuk/giri\\_processing/tree/master/archaeo\\_morphology\\_clicking](https://github.com/rmanzuk/giri_processing/tree/master/archaeo_morphology_clicking)

**ORCID**

- Ryan A. Manzuk  <https://orcid.org/0000-0002-3073-9493>  
Adam C. Maloof  <https://orcid.org/0000-0003-0032-6628>  
Jaap A. Kaandorp  <https://orcid.org/0000-0003-4558-7135>  
Mark Webster  <https://orcid.org/0000-0002-4995-9103>

**REFERENCES**

- Al-Horani, F. A., Al-Moghrabi, S. M., & de Beer, D. (2003). The mechanism of calcification and its relation to photosynthesis and respiration in the scleractinian coral *Galaxea fascicularis*. *Marine Biology*, 142, 419–426.
- Antcliffe, J. B., Callow, R. H. T., & Brasier, M. D. (2014). Giving the early fossil record of sponges a squeeze. *Biological Reviews*, 89, 972–1004.
- Antcliffe, J. B., Jessop, W., & Daley, A. C. (2019). Prey fractionation in the Archaeocyatha and its implication for the ecology of the first animal reef systems. *Paleobiology*, 45, 652–675.
- Asadzadeh, S. S., Kiørboe, T., Larsen, P. S., Leys, S. P., Yahel, G., & Walther, J. H. (2020). Hydrodynamics of sponge pumps and evolution of the sponge body plan. *eLife*, 9, e61012.
- Berkner, L. V., & Marshall, L. C. (1965). On the origin and rise of oxygen concentration in the Earth's atmosphere. *Journal of the Atmospheric Sciences*, 22, 225–261.
- Bobrovskiy, I., Hope, J. M., Nettersheim, B. J., Volkman, J. K., Hallmann, C., & Brocks, J. J. (2021). Algal origin of sponge sterane biomarkers negates the oldest evidence for animals in the rock record. *Nature Ecology & Evolution*, 5, 165–168.
- Botting, J. P., & Muir, L. A. (2018). Early sponge evolution: A review and phylogenetic framework. *Palaeoworld*, 27, 1–29.
- Bottjer, D. J., Hagadorn, J. W., & Dornbos, S. Q. (2000). The Cambrian substrate revolution. *GSA Today*, 10, 1–7.
- Brain, C., Prave, A. R., Herd, D. A., Allison, S. G., Hoffmann, K.-H., Fallick, A. E., Botha, A., Sturrock, C., Young, I., & Condon, D. J. (2012). The first animals: ca. 760-million-year-old sponge-like fossils from Namibia. *South African Journal of Science*, 108, 1–8.
- Brasier, M. D., & Lindsay, J. F. (2001). Did supercontinental amalgamation trigger the "Cambrian Explosion". In *The Ecology of the Cambrian Radiation* (pp. 69–89). Columbia University Press.
- Brooke, N. M., Garcia-Fernández, J., & Holland, P. W. H. (1998). The ParaHox gene cluster is an evolutionary sister of the Hox gene cluster. *Nature*, 392, 920–922.
- Canfield, D. E., Poulton, S. W., & Narbonne, G. M. (2007). Late-Neoproterozoic deep-ocean oxygenation and the rise of animal life. *Science*, 315, 92–95.
- Cantine, M. D., Knoll, A. H., & Bergmann, K. D. (2020). Carbonates before skeletons: A database approach. *Earth-Science Reviews*, 201, 103065.
- Catling, D. C., Glein, C. R., Zahnle, K. J., & McKay, C. P. (2005). Why O<sub>2</sub> is required by complex life on habitable planets and the concept of planetary "oxygenation time.". *Astrobiology*, 5, 415–438.
- Cloud, P. E. (1968). Pre-metazoan evolution and the origins of the Metazoa. *Evolution and Environment*, 72, 1–72.
- Cordie, D. R., Dornbos, S. Q., Marenco, P. J., Oji, T., & Gonchigdorj, S. (2019). Depauperate skeletonized reef-dwelling fauna of the early Cambrian: Insights from archaeocyathan reef ecosystems of western Mongolia. *Palaeogeography, Palaeoclimatology, Palaeoecology*, 514, 206–221.
- Cowan, C. A., & James, N. P. (1993). The interactions of sea-level change, terrigenous-sediment influx, and carbonate productivity as controls on Upper Cambrian Grand Cycles of western Newfoundland, Canada. *Geological Society of America Bulletin*, 105, 1576–1590.
- Cracknell, K., García-Bellido, D. C., Gehling, J. G., Ankor, M. J., Darroch, S. A. F., & Rahman, I. A. (2021). Pentaradial eukaryote suggests expansion of suspension feeding in White Sea-aged Ediacaran communities. *Scientific Reports*, 11, 1–9.
- Dahl, T. W., Connelly, J. N., Li, D., Kouchinsky, A., Gill, B. C., Porter, S., Maloof, A. C., & Bizzarro, M. (2019). Atmosphere–ocean oxygen and productivity dynamics during early animal radiations. *Proceedings of the National Academy of Sciences*, 116, 19352–19361.
- Debrenne, F. (2007). Lower Cambrian archaeocyathan bioconstructions. *Comptes Rendus Palevol*, 6, 5–19.
- Debrenne, F., & Zhuravlev, A. (1992). *Irregular archaeocyaths: Morphology, ontogeny, systematics, biostratigraphy, palaeoecology*. Editions du CNRS.
- Dilliard, K. A., Pope, M. C., Coniglio, M., Hasiotis, S. T., & Lieberman, B. S. (2007). Stable isotope geochemistry of the lower Cambrian Sekwi Formation, Northwest Territories, Canada: Implications for ocean chemistry and secular curve generation. *Palaeogeography, Palaeoclimatology, Palaeoecology*, 256, 174–194.
- Domeier, M. (2018). Early Paleozoic tectonics of Asia: Towards a full-plate model. *Geoscience Frontiers*, 9, 789–862.
- Droser, M. L., & Gehling, J. G. (2015). The advent of animals: the view from the Ediacaran. *Proceedings of the National Academy of Sciences*, 112, 4865–4870.
- Erpenbeck, D., Sutcliffe, P., de Cook, S. C., Dietzel, A., Maldonado, M., van Soest, R. W. M., JNA, H., & Wörheide, G. (2012). Horn sponges and their affairs: On the phylogenetic relationships of kerato sponges. *Molecular Phylogenetics and Evolution*, 63, 809–816.
- Erpenbeck, D., & van Soest, R. W. M. (2002). Halichondriidae Gray, 1867. In J. N. Hooper & R. W. M. van Soest (Eds.), *Systema Porifera: A guide to the classification of sponges* (pp. 783–815). Kluwer Academic/Plenum Publishers.
- Erwin, D. H., & Valentine, J. W. (2012). *The Cambrian explosion: The construction of animal biodiversity*. Roberts.
- Erwin, D. H., & Tweedt, S. (2012). Ecological drivers of the Ediacaran–Cambrian diversification of Metazoa. *Evolutionary Ecology*, 26(2), 417–433.
- Faggetter, L. E., Wignall, P. B., Pruss, S. B., Jones, D. S., Grasby, S., Widdowson, M., & Newton, R. J. (2019). Mercury chemostratigraphy across the Cambrian Series 2-Series 3 boundary: Evidence for increased volcanic activity coincident with extinction? *Chemical Geology*, 510, 188–199.
- Farji-Brener, A. G., Chinchilla, F., Umaña, M. N., Ocasio-Torres, M. E., Chauta-Mellizo, A., Acosta-Rojas, D., Marinaro, S., de Torres Curth, M., & Amador-Vargas, S. (2015). Branching angles reflect a trade-off between reducing trail maintenance costs or travel distances in leaf-cutting ants. *Ecology*, 96, 510–517.
- Filatov, M. V., Kaandorp, J. A., Postma, M., van Liere, R., Kruszyński, K. J., Vermeij, M. J. A., Streekstra, G. J., & RPM, B. (2010). A comparison between coral colonies of the genus *Madracis* and simulated forms. *Proceedings of the Royal Society B: Biological Sciences*, 277, 3555–3561.
- Filatov, M. V., Frade, P. R., RPM, B., MJA, V., & Kaandorp, J. A. (2013). Comparison between colony morphology and molecular phylogeny in the Caribbean scleractinian coral genus *Madracis*. *PLoS One*, 8, e71287.
- Getraer, A., & Maloof, A. C. (2021). Climate-driven variability in runoff erosion encoded in stream network geometry. *Geophysical Research Letters*, 48, e2020GL091777.
- Geyman, E. C., & Maloof, A. C. (2019). A diurnal carbon engine explains <sup>13</sup>C-enriched carbonates without increasing the global production of oxygen. *Proceedings of the National Academy of Sciences*, 116, 24433–24439.
- Geyman, E. C., & Maloof, A. C. (2021). Facies control on carbonate δ<sup>13</sup>C on the Great Bahama Bank. *Geology*, 49, 1049–1054.
- Goreau, T. F. (1959). The physiology of skeleton formation in corals. I. A method for measuring the rate of calcium deposition by corals under different conditions. *The Biological Bulletin*, 116, 59–75.
- Griffiths, J. R., Kadin, M., Nascimento, F. J. A., Tamelander, T., Törnroos, A., Bonaglia, S., Bonsdorff, E., Brüchert, V., Gårdmark, A., & Järnström, M. (2017). The importance of benthic–pelagic coupling

- for marine ecosystem functioning in a changing world. *Global Change Biology*, 23, 2179–2196.
- Hatcher, B. G. (1988). Coral reef primary productivity: a beggar's banquet. *Trends in Ecology & Evolution*, 3, 106–111.
- Hicks, M. K. (2001). *Paleoecology of Upper Harkless archaeocythan reefs in Esmeralda County, Nevada*. University of Nevada.
- Hollingsworth, J. S. (2011). Lithostratigraphy and biostratigraphy of Cambrian Stage 3 in western Nevada and eastern California. *Museum of Northern Arizona Bulletin*, 67, 26–42.
- Howes, B., Mehra, A., & Maloof, A. (2021). Three-dimensional morphometry of ooids in oolites: A new tool for more accurate and precise paleoenvironmental interpretation. *Journal of Geophysical Research: Earth Surface*, 126(4), e2020JF005601.
- Hubbard, D. K., Gill, I. P., & Burke, R. B. (2001). The role of framework in modern reefs and its application to ancient systems. In *The history and sedimentology of ancient reef systems* (pp. 351–386). Springer.
- Hubbard, D. K., Miller, A. I., & Scaturo, D. (1990). Production and cycling of calcium carbonate in a shelf-edge reef system (St. Croix, US Virgin Islands); applications to the nature of reef systems in the fossil record. *Journal of Sedimentary Research*, 60, 335–360.
- Idjadi, J. A., & Edmunds, P. J. (2006). Scleractinian corals as facilitators for other invertebrates on a Caribbean reef. *Marine Ecology Progress Series*, 319, 117–127.
- James, N. P., & Kobluk, D. R. (1978). Lower Cambrian patch reefs and associated sediments: Southern Labrador, Canada. *Sedimentology*, 25, 1–35.
- James, N. P., Kobluk, D. R., & Pemberton, S. G. (1977). The oldest macroborers: lower Cambrian of Labrador. *Science*, 197, 980–983.
- James, N. P., & Mountjoy, E. W. (1983). Shelf-slope break in fossil carbonate platforms: an overview. In D. J. Stanley & G. T. Moore (Eds.), *The shelf-break: Critical interface on continental margins* (pp. 189–206). Society of Economic Paleontologists and Mineralogists Special Publications.
- Kaandorp, J. A. (1999). Morphological analysis of growth forms of branching marine sessile organisms along environmental gradients. *Marine Biology*, 134, 295–306.
- Kaandorp, J. A. (2013). Macroscopic modelling of environmental influence on growth and form of sponges and corals using the accretive growth model. *International Scholarly Research Notices*, 2013, 1–14.
- Kaandorp, J. A., & Kübler, J. E. (2001). *The algorithmic beauty of seaweeds, sponges and corals*. Springer Science & Business Media.
- Kaandorp, J. A., Sloot, P. M. A., Merks, R. M. H., Bak, R. P. M., Vermeij, M. J. A., & Maier, C. (2005). Morphogenesis of the branching reef coral *Madracis mirabilis*. *Proceedings of the Royal Society B: Biological Sciences*, 272, 127–133.
- Karlstrom, K., Hagadorn, J., Gehrels, G., Matthews, W., Schmitz, M., Madronich, L., Mulder, J., Pecha, M., Giesler, D., & Crossey, L. (2018). Cambrian Sauk transgression in the Grand Canyon region redefined by detrital zircons. *Nature Geoscience*, 11, 438–443.
- Karlstrom, K. E., Mohr, M. T., Schmitz, M. D., Sundberg, F. A., Rowland, S. M., Blakey, R., Foster, J. R., Crossey, L. J., Dehler, C. M., & Hagadorn, J. W. (2020). Redefining the Tonto Group of Grand Canyon and recalibrating the Cambrian time scale. *Geology*, 48, 425–430.
- Kerans, C., & Tinker, S. W. (1999). Extrinsic stratigraphic controls on development of the Capitan reef complex. In *Geologic Framework of the Capitan Reef*. SEPM Society for Sedimentary Geology.
- Kiessling, W. (2005). Habitat effects and sampling bias on Phanerozoic reef distribution. *Facies*, 51, 24–32.
- Kiessling, W. (2006). Towards an unbiased estimate of fluctuations in reef abundance and volume during the Phanerozoic. *Biogeosciences*, 3, 15–27.
- Kiessling, W., & Flügel, E. (2002). Paleoreefs—A database on Phanerozoic reefs. In *Phanerozoic reef patterns* (pp 77–92). SEPM (Society for Sedimentary Geology).
- Kiessling, W., Simpson, C., & Foote, M. (2010). Reefs as cradles of evolution and sources of biodiversity in the Phanerozoic. *Science*, 327, 196–198.
- Kobluk, D. R., & James, N. P. (1979). Cavity-dwelling organisms in Lower Cambrian patch reefs from southern Labrador. *Lethaia*, 12, 193–218.
- Kobluk, D. R. (1988). Cryptic faunas in reefs; ecology and geologic importance. *PALAIOS*, 3, 379–390.
- Kostylev, V. E., Erlandsson, J., Ming, M. Y., & Williams, G. A. (2005). The relative importance of habitat complexity and surface area in assessing biodiversity: Fractal application on rocky shores. *Ecological Complexity*, 2, 272–286.
- Kruszyński, K. J., Kaandorp, J. A., & van Liere, R. (2007). A computational method for quantifying morphological variation in scleractinian corals. *Coral Reefs*, 26, 831–840.
- Laflamme, M., Darroch, S. A. F., Tweedt, S. M., Peterson, K. J., & Erwin, D. H. (2013). The end of the Ediacara biota: Extinction, biotic replacement, or Cheshire Cat? *Gondwana Research*, 23, 558–573.
- Land, L. S. (1979). The fate of reef-derived sediment on the north Jamaican Island slope. *Marine Geology*, 29, 55–71.
- Levinton, J. (1972). Stability and trophic structure in deposit-feeding and suspension-feeding communities. *The American Naturalist*, 106, 472–486.
- Lidz, B. H., Reich, C. D., Peterson, R. L., & Shinn, E. A. (2006). New maps, new information: Coral reefs of the Florida Keys. *Journal of Coastal Research*, 22, 260–282.
- Lipps, J. H., & Signor, P. W. (1992). *Origin and early evolution of the Metazoa [Topics in Geobiology]*. Plenum Press.
- Love, G. D., Grosjean, E., Stalvies, C., Fike, D. A., Grotzinger, J. P., Bradley, A. S., Kelly, A. E., Bhatia, M., Meredith, W., Snape, C. E., & Bowring, S. A. (2009). Fossil steroids record the appearance of Demospongiae during the Cryogenian period. *Nature*, 457, 718–721.
- Love, G. D., & Summons, R. E. (2015). The molecular record of Cryogenian sponges—A response to Antcliffe (2013). *Palaeontology*, 58, 1131–1136.
- Lowe, R. J., Koseff, J. R., & Monismith, S. G. (2005). Oscillatory flow through submerged canopies: 1. Velocity structure. *Journal of Geophysical Research: Oceans*, 110.
- Lowe, R. J., Koseff, J. R., Monismith, S. G., & Falter, J. L. (2005). Oscillatory flow through submerged canopies: 2. Canopy mass transfer. *Journal of Geophysical Research: Oceans*, 110.
- Maloof, A. C., Rose, C. V., Beach, R., Samuels, B. M., Calmet, C. C., Erwin, D. H., Poirier, G. R., Yao, N., & Simons, F. J. (2010). Possible animal-body fossils in pre-Marinoan limestones from South Australia. *Nature Geoscience*, 3, 653–659.
- Marshall, C. R., & Valentine, J. W. (2010). The importance of preadapted genomes in the origin of the animal bodyplans and the Cambrian explosion. *Evolution: International Journal of Organic Evolution*, 64, 1189–1201.
- Maxwell, W. G. H., Day, R. W., & Fleming, P. J. G. (1961). Carbonate sedimentation on the Heron Island reef, Great Barrier reef. *Journal of Sedimentary Research*, 31, 215–230.
- Mehra, A., & Maloof, A. (2018). Multiscale approach reveals that *Cloudina* aggregates are detritus and not *in situ* reef constructions. *Proceedings of the National Academy of Sciences*, 115, 201719911.
- Mehra, A., Watters, W. A., Grotzinger, J. P., & Maloof, A. C. (2020). Three-dimensional reconstructions of the putative metazoan *Namapoikia* show that it was a microbial construction. *Proceedings of the National Academy of Sciences*, 117, 19760–19766.
- Meysman, F. J. R., Middelburg, J. J., & Heip, C. H. R. (2006). Bioturbation: A fresh look at Darwin's last idea. *Trends in Ecology & Evolution*, 21, 688–695.
- Monismith, S. G. (2007). Hydrodynamics of coral reefs. *Annual Review of Fluid Mechanics*, 39, 37–55.
- Montañez, I. P., Osleger, D. A., Banner, J. L., Mack, L. E., & Musgrave, M. (2000). Evolution of the Sr and C isotope composition of Cambrian oceans. *GSA Today*, 10, 1–7.

- Muko, S., Kawasaki, K., Sakai, K., Takasu, F., & Shigesada, N. (2000). Morphological plasticity in the coral *Porites sillimaniiana* and its adaptive significance. *Bulletin of Marine Science*, 66, 225–239.
- Peng, S. C., Babcock, L. E., & Ahlberg, P. (2020). The Cambrian period. In *Geologic time scale 2020* (pp. 565–629). Elsevier.
- Penny, A. M., Wood, R., Curtis, A., Bowyer, F., Tostevin, R., & Hoffman, K.-H. (2014). Ediacaran metazoan reefs from the Nama Group, Namibia. *Science*, 344, 1504–1506.
- Peters, S. E., & Gaines, R. R. (2012). Formation of the 'Great Unconformity' as a trigger for the Cambrian explosion. *Nature*, 484, 363–366.
- Peterson, K. J., Dietrich, M. R., & McPeek, M. A. (2009). MicroRNAs and metazoan macroevolution: insights into canalization, complexity, and the Cambrian explosion. *BioEssays*, 31, 736–747.
- Petroff, A. P., Devauchelle, O., Abrams, D. M., Lobkovsky, A. E., Kudrolli, A., & Rothman, D. H. (2011). Geometry of valley growth. *Journal of Fluid Mechanics*, 673, 245–254.
- Playford, P. E. (1980). Devonian "Great Barrier Reef" of Canning Basin, Western Australia. *AAPG Bulletin*, 64, 814–840.
- Pratt, B. R., Spincer, B. R., Wood, R. A., & Zhuravlev, A. Y. (2001). Ecology and evolution of Cambrian reefs. In *The ecology of the Cambrian radiation* (pp. 254–274). Columbia University Press.
- Pruss, S. B., Clemente, H., & Laflamme, M. (2012). Early (Series 2) Cambrian archaeocyathan reefs of southern Labrador as a locus for skeletal carbonate production. *Lethaia*, 45, 401–410.
- Pruss, S. B., Slaymaker, M. L., Smith, E. F., Zhuravlev, A. Y., & Fike, D. A. (2021). Cambrian reefs in the lower Poleta Formation: a new occurrence of a thick archaeocyathan reef near Gold Point, Nevada, USA. *Facies*, 67(2), 1–13.
- Purdy, E. G., & Gischler, E. (2003). The Belize margin revisited: 1. Holocene marine facies. *International Journal of Earth Sciences*, 92, 532–551.
- Read, B. C. (1980). Lower Cambrian archeocyathid buildups, Pelly Mountains, Yukon. *Geological Survey of Canada Paper*, 78-18, 54.
- Reaka-Kudla, M. L. (1997). The global biodiversity of coral reefs: A comparison with rain forests. *Biodiversity II: Understanding and Protecting our Biological Resources*, 2, 551.
- Rees, M. N., Pratt, B. R., & Rowell, A. J. (1989). Early Cambrian reefs, reef complexes, and associated lithofacies of the Shackleton Limestone, Transantarctic Mountains. *Sedimentology*, 36, 341–361.
- Reidenbach, M. A., Koseff, J. R., Monismith, S. G., Steinbuck, J. V., & Genin, A. (2006). The effects of waves and morphology on mass transfer within branched reef corals. *Limnology and Oceanography*, 51, 1134–1141.
- Reitner, J., & Wörheide, G. (2002). Non-lithistid fossil Demospongiae—Origins of their palaeobiodiversity and highlights in history of preservation. In *Systema Porifera* (pp. 52–68). Springer.
- Richter, C., & Wunsch, M. (1999). Cavity-dwelling suspension feeders in coral reefs—A new link in reef trophodynamics. *Marine Ecology Progress Series*, 188, 105–116.
- Rowland, S. M. (1984). Were there framework reefs in the Cambrian? *Geology*, 12, 181–183.
- Rowland, S. M. (2001). Archaeocyaths—A history of phylogenetic interpretation. *Journal of Paleontology*, 75, 1065–1078.
- Rowland, S. M., & Gangloff, R. A. (1988). Structure and paleoecology of Lower Cambrian reefs. *PALAIOS*, 3, 111–135.
- Rowland, S. M., Oliver, L. K., Hicks, M., Duebendorfer, E. M., & Smith, E. I. (2008). Ediacaran and early Cambrian reefs of Esmeralda County, Nevada: non-congruent communities within congruent ecosystems across the Neoproterozoic–Paleozoic boundary. *Field Guide to Plutons, Volcanoes, Faults, Reefs, Dinosaurs, and Possible Glaciation in Selected Areas of Arizona, California, and Nevada: Geological Society of America Field Guide*, 11, 83–100.
- Rowland, S. M., & Shapiro, R. S. (2002). Reef patterns and environmental influences in the Cambrian and earliest Ordovician. In W. Kiessling, E. Flügel, & J. Golonka (Eds.), *Phanerozoic reef patterns* (pp. 95–128). SEPM Society for Sedimentary Geology.
- Roy, A. G. (1983). Optimal angular geometry models of river branching. *Geographical Analysis*, 15, 87–96.
- Roy, A. G., & Woldenberg, M. J. (1982). A generalization of the optimal models of arterial branching. *Bulletin of Mathematical Biology*, 44, 349–360.
- Sagy, A., Reches, Z., & Roman, I. (2001). Dynamic fracturing: field and experimental observations. *Journal of Structural Geology*, 23, 1223–1239.
- Sanna, G., & Freiwald, A. (2021). Deciphering the composite morphological diversity of *Lophelia pertusa*, a cosmopolitan deep-water ecosystem engineer. *Ecosphere*, 12, e03802.
- Schiffbauer, J. D., Selly, T., Jacquet, S. M., Merz, R. A., Nelson, L. L., Strange, M. A., Cai, Y., & Smith, E. F. (2020). Discovery of bilaterian-type through-guts in claudinomorphs from the terminal Ediacaran Period. *Nature Communications*, 11, 1–12.
- Shaish, L., Abelson, A., & Rinkevich, B. (2007). How plastic can phenotypic plasticity be? The branching coral *Stylophora pistillata* as a model system. *PLoS One*, 2, e644.
- Shashar, N., Kinane, S., Jokiel, P. L., & Patterson, M. R. (1996). Hydromechanical boundary layers over a coral reef. *Journal of Experimental Marine Biology and Ecology*, 199, 17–28.
- Signor, P. W. (1990). The geologic history of diversity. *Annual Review of Ecology and Systematics*, 21, 509–539.
- Skovsted, C. B., Balthasar, U., Vinther, J., & Sperling, E. A. (2021). Small shelly fossils and carbon isotopes from the early Cambrian (Stages 3–4) Mural Formation of western Laurentia. *Papers in Palaeontology*, 7, 951–983.
- Sperling, E. A., Robinson, J. M., Pisani, D., & Peterson, K. J. (2010). Where's the glass? Biomarkers, molecular clocks, and microRNAs suggest a 200-Myr missing Precambrian fossil record of siliceous sponge spicules. *Geobiology*, 8, 24–36.
- Squire, R. J., Campbell, I. H., Allen, C. M., & Wilson, C. J. L. (2006). Did the Transgondwanan Supermountain trigger the explosive radiation of animals on Earth? *Earth and Planetary Science Letters*, 250, 116–133.
- Sundberg, F. A., Karlstrom, K. E., Geyer, G., Foster, J. R., Hagadorn, J. W., Mohr, M. T., Schmitz, M. D., Dehler, C. M., & Crossey, L. J. (2020). Asynchronous trilobite extinctions at the early to middle Cambrian transition. *Geology*, 48, 441–445.
- Surge, D. M., Savarese, M., Robert Dodd, J., & Lohmann, K. C. (1997). Carbon isotopic evidence for photosynthesis in early Cambrian oceans. *Geology*, 25, 503–506.
- Thomas, F. I. M., & Atkinson, M. J. (1997). Ammonium uptake by coral reefs: Effects of water velocity and surface roughness on mass transfer. *Limnology and Oceanography*, 42, 81–88.
- Todd, P. A. (2008). Morphological plasticity in scleractinian corals. *Biological Reviews*, 83, 315–337.
- Torsvik, T. H., & Cocks, L. R. M. (2016). *Earth history and palaeogeography*. Cambridge University Press.
- Turner, E. C. (2021). Possible poriferan body fossils in early Neoproterozoic microbial reefs. *Nature*, 596, 87–91.
- Vacelet, J. (2002). Recent 'Sphinctozoa', Order Verticillitida, Family Verticillitidae Steinmann, 1882. In *Systema Porifera* (pp. 1097–1098). Springer.
- Valentine, J. W. (1986). Fossil record of the origin of Baupläne and its implications. In *Patterns and processes in the history of life* (pp. 209–222). Springer.
- Valentine, J. W. (1995). Why no new phyla after the Cambrian? Genome and ecospace hypotheses revisited. *PALAIOS*, 10, 190–194.
- Valentine, J. W., & Moores, E. M. (1972). Global tectonics and the fossil record. *The Journal of Geology*, 80, 167–184.
- Vermeij, G. J. (1989). The origin of skeletons. *PALAIOS*, 4, 585–589.
- Vytopil, E., & Willis, B. (2001). Epifaunal community structure in *Acropora* spp. (Scleractinia) on the Great Barrier Reef: implications of coral morphology and habitat complexity. *Coral Reefs*, 20, 281–288.
- Walter, M. R. (1976). *Stromatolites*. Elsevier.

- Watters, W. A., & Grotzinger, J. P. (2001). Digital reconstruction of calcified early metazoans, terminal Proterozoic Nama Group, Namibia. *Paleobiology*, 27, 159–171.
- Wood, R. (1993). Nutrients, predation and the history of reef-building. *PALAIOS*, 8(6), 526–543.
- Wood, R. (1995). The changing biology of reef-building. *PALAIOS*, 10(6), 517–529.
- Wood, R. (1999). *Reef evolution*. Oxford University Press on Demand.
- Wood, R., & Curtis, A. (2015). Extensive metazoan reefs from the Ediacaran Nama Group, Namibia: The rise of benthic suspension feeding. *Geobiology*, 13, 112–122.
- Wood, R. A., Zhuravlev, A. Y., & Debrenne, F. (1992). Functional biology and ecology of Archaeocyatha. *PALAIOS*, 7, 131–156.
- Wotte, T., Strauss, H., & Sundberg, F. A. (2011). Carbon and sulfur isotopes from the Cambrian Series 2–Cambrian Series 3 of Laurentia and Siberia. *Museum of Northern Arizona Bulletin*, 67, 43–63.
- Yuan, X., Chen, Z., Xiao, S., Zhou, C., & Hua, H. (2011). An early Ediacaran assemblage of macroscopic and morphologically differentiated eukaryotes. *Nature*, 470, 390–393.
- Zhuravlev, A. Y. (2001). Paleoecology of Cambrian reef ecosystems. In *The history and sedimentology of ancient reef systems* (pp. 121–157). Springer.
- Zhuravlev, A. Y. (2015). The early history of the Metazoa—A paleontologist's viewpoint. *Biology Bulletin Reviews*, 5, 415–461.
- Zhuravlev, A. Y., & Naimark, E. B. (2005). Alpha, beta, or gamma? Numerical view on the early Cambrian world. *Palaeogeography, Palaeoclimatology, Palaeoecology*, 220, 207–225.
- Zhuravlev, A. Y., Naimark, E. B., & Wood, R. A. (2015). Controls on the diversity and structure of earliest metazoan communities: early Cambrian reefs from Siberia. *Earth-Science Reviews*, 147, 18–29.
- Zhuravlev, A. Y., & Riding, R. (2001). *The ecology of the Cambrian radiation*. Columbia University Press.
- Zhuravlev, A. Y., & Wood, R. (1995). Lower Cambrian reefal cryptic communities. *Palaeontology*, 38, 443–470.

**How to cite this article:** Manzuk, R. A., Maloof, A. C., Kaandorp, J. A., & Webster, M. (2023). Branching archaeocyaths as ecosystem engineers during the Cambrian radiation. *Geobiology*, 21, 66–85. <https://doi.org/10.1111/gbi.12521>